[Frontiers in Bioscience, Elite, 25, 299-334, Jan 1, 2020]

A new backpropagation neural network classification model for prediction of incidence of malaria

Ajeet Kumar Verma[1], Venkatanareshbabu Kuppili[1], Saurabh K. Srivastava[2], Jasjit S. Suri[2,3]

[1]Department of Computer Science and Engineering, NIT Goa, India, [2]Advanced Knowledge Engineering Center, Global Biomedical Technologies, Inc., Roseville, CA, USA, [3]AtheroPoint™, Roseville, CA, USA

TABLE OF CONTENTS

1. Abstract
2. Introduction
    2.1 Lifecycle of malaria
3. Derivation of the proposed model
    3.1. Proposed System
    3.2. Nonlinear integrate-and-fire neuron model
    3.3. Proposed spiking model
    3.4. Interspike interval and firing rate of the proposed spiking model
    3.5. construction of a new aggregation function
    3.6. Proposed ISI-BPNN and training algorithm
        3.6.1. Construction of the proposed isi-based backpropagation (ISI-BP)
4. Machine learning architecture
    4.1. Conventional classifiers
        4.1.1. Multilayer perceptron
        4.1.2. Support vector machine
        4.1.3. Generalized-constraint neural network
5. Data collection and experimental protocol
    5.1. Data collection
        5.1.1. Demographics, recording protocol and ground truth
        5.1.2. Meteorological data
        5.1.3. Geographical location of villages
        5.1.4. Ethics approval
    5.2. Experiment 1: computation of accuracy of ISI-BPNN using K2 and K10 cross-validation
    5.3. Experiment 2: effect of training set Using ISI-BPNN for dataset
    5.4. Experiment 3: inter-classifier comparison
6. Results
    6.1. Results of experiment 1
    6.2. Results of experiment 2
    6.3. Results of experiment 3
7. Performance evaluation
    7.1. The Receiver Operating Characteristic Curve
    7.2. Sensitivity Analysis
8. Scientific validation
    8.1. Malaria segregation index (MSI)

8.1.1. Index of dissimilarity
8.1.2. Isolation index of segregation
8.1.3. Exposure or interaction measure of segregation
8.1.4. Odds ratio and risk ratio analysis
8.2. Validation on thoracic data
8.3. Validation on parkinson's dataset
9. Discussion
9.1. Benchmarking
9.2. A Special note on the sigmoid function
9.3. A Note on spiking neuron models
9.4. Strengths, weaknesses and extensions
10. Conclusions
11. Acknowledgment
12. References

1. ABSTRACT

Malaria is an infectious disease caused by parasitic protozoans of the Plasmodium family. These parasites are transmitted by mosquitos which are common in certain parts of the world. Based on their specific climates, these regions have been classified as low and high risk regions using a backpropagation neural network (BPNN). However, this approach yielded low performance and stability necessitating development of a more robust model. We hypothesized that by spiking neuron models in simulating the characteristics of a neuron, which when embedded with a BPNN, could improve the performance for the assessment of malaria prone regions. To this end, we created an inter-spike interval (ISI)-based BPNN (ISI-BPNN) architecture that uses a single-pass spiking learning strategy and has a parallel structure that is useful for non-linear regression tasks. Existing malaria dataset comprised of 1296 records, that met these attributes, were used. ISI-BPNN showed superior performance, and a high accuracy. The benchmarking results showed reliability and stability and an improvement of 11.9% against a multilayer perceptron and 9.19% against integrate-and-fire neuron models. The ISI-BPNN model is well suited for deciphering the risk of acquiring malaria as well as other diseases in prone regions of the world.

2. INTRODUCTION

Malaria is a life threatening mosquito-borne infectious disease that exists in almost all nations. Almost half of the world's population is at risk of malaria (1). The epidemiological patterns of malaria have been changing globally. The World Health Organization (WHO)'s world malaria report of 2018 stated that there were 219 million malaria cases worldwide and a total of 435,000 estimated deaths in 2017 (2). Southern Africa has the highest share of global malaria, with 194 million malaria cases and 407,000 deaths. High rates were also seen in the Asia Pacific region: Myanmar had 962,000 malaria cases with 2880 deaths, India 105,000 malaria cases and 690 deaths, and Indonesia 105,000 malaria cases and 1230 deaths as shown in Table 1. Ashwani *et al*. (3) reported on the malaria statistics in India, finding 4,481 confirmed deaths (medically certified) and an estimated 49,796 deaths (unconfirmed death reports). The authors gave statistics for Orissa (a state in the west of India) with almost 96,000 malaria cases and 1,793 deaths; for Madhya Pradesh (central India), these Figures were 50,000 malaria cases with 890 deaths, and in Karnataka (southern India) 82,000 malaria cases with 407 deaths. The authors further stated that adult and child cases gave rise to 2,681 malaria deaths; 90% were in rural areas, and 86% were due to a lack of medical facilities. Walther *et al*. (4) presented a survey of quantitative epidemiology methods and addressed global challenges to the worldwide elimination of malaria. Darkoh *et al.* (5) developed a water-based prediction model for the prediction of malaria prevalence in Ameni, in the west of Ghana.

Table 1. Worldwide incidence and mortality of malaria

Global burden (2016-2017)			
SN	**Region**	**Cases**	**Deaths**
1	African	194 million	407000
2	South-East Asia	14.6 million	27000
3	Eastern Mediterranean	4.3 million	8200
Asia (2016-2017)			
1	Myanmar	962610	2880
2	India	8760000	690
3	Indonesia	105890	1230
4	Thailand	35810	120
5	Bangladesh	34400	550
India (2016-2017)			
1	Orissa	962610	1793
2	Madhya Pradesh	508800	890
3	Karnataka	822560	407
4	Maharashtra	339200	326
5	Gujarat	37028	212

Malaria is caused by a family of parasitic protozoans of the Plasmodium family. The Plasmodium parasite has several different species, but only five are responsible for malaria infection: Falciparum, Vivax, Malariae, Ovale, and Knowlesi. In India, the first two of these species cause malaria in humans. The dominant infecting species is Vivax; however, there was a reduction in its prevalence in 1985, which brought the ratio of Falciparum to Vivax to 0.41. In 1995, the ratio increased to 0.60 and this had changed to 1.01 by 2010 (6). The WHO launched a project of prevention and control of malaria disease in India, and the current work was carried out under their aegis (1). Certain geographical regions are more affected than others by the number of patients and by climatic conditions, which are dependent on attributes such as temperature, humidity and rainfall, it is therefore necessary to classify these regions into low or high-risk areas for malaria. By classifying malaria-prone zones, we can obtain information about high-risk areas, which can then be reported to the municipal authorities and other local bodies. These organizations can use this information to prevent this disease by initiating early fogging and other control measures to stop the breeding of malaria species. Our objective is therefore to classify regions of high or low proneness to malaria, based on climatic conditions and their changes. This study is focused on the identification of malaria-prone zones and on the triggers for the occurrence of malaria in a specific geographic location in Goa, India.

2.1 Lifecycle of Malaria

Malaria is usually transmitted by a female mosquito (7)(8). Malaria is also communicable through the bite of the mosquito. When, an infected Anopheles mosquito bites, it introduces parasite to our blood. Also, when a mosquito bites an infected person, biting mosquito becomes infected and it transmits the parasite. The parasite, present in Anopheles saliva, enters the blood through the bite. Through the bloodstream, parasite reaches to the liver. Parasite matures and reproduces in the liver within 48 to 72 hours (9)(10). The matured parasite then travels through the bloodstream, and starts infecting the blood cells, usually RBC. Once parasite enters into RBC, it starts multiplying within two to three days, causing the burst of a cell, and as a result, this infection is transmitted to other cells in the blood. At synchronous time intervals, infected blood cells burst and it introduces more population of parasites in the blood. The bursting cycle of infected blood cells

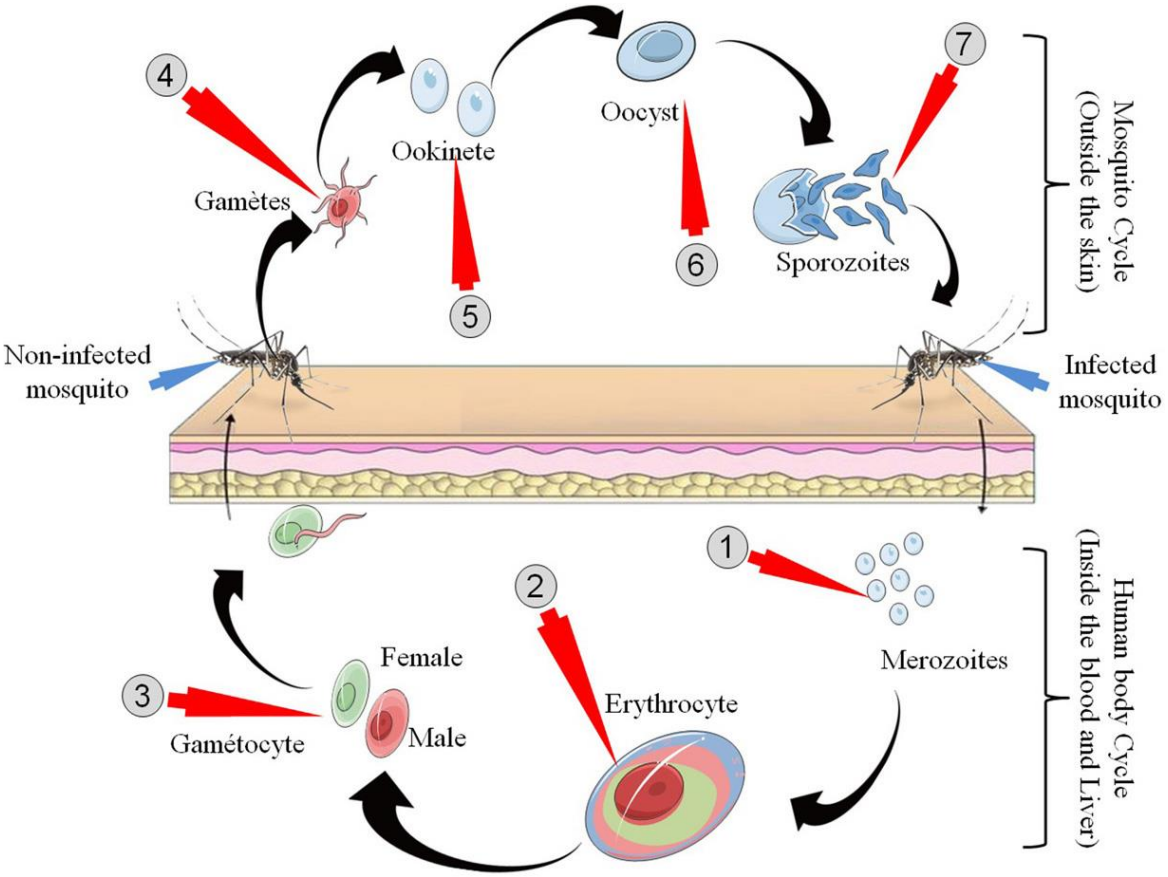

Figure 1. Malaria parasite life cycle.

is 48-72 hours. Each time when cells are bursting, a person feels a bout of fever, sweating and chills. Malaria parasite infection cycle is shown in Figure 1. The parasites persuade separation of the infected hepatocyte takes place, enabling it to relocate to the liver sinusoid where sprouting of parasite-filled vesicles called merosomes (Figure 1: Label 1). The new merozoites rapidly divide within erythrocytes, sometimes synchronously in cycles with fever and chills (Figure 1: Label 2). Responding to an unconfirmed cue, few parasites separate into male and female gametocytes (Figure 1: Label 3), which are the forms that live inactively in the circulatory system for a week. When gametocyte enters the mosquito by means of blood, they quickly transit to become initiated male and female gametes (Figure 1: Label 4). The motile and fleeting diploid parasite frame, the ookinete, moves out of the blood (Figure 1: Label 5), over the peritrophic lattice to the mid-gut partition where an oocyst is shaped (Figure 1: Label 6). After a meiotic decrease in the chromosome, numbers of sporozoites are framed inside the oocyst (Figure 1: Label 7). Finally, the oocyst splits and sporozoites relocate to the salivary organ to anticipate exchange with vertebrate host. Malaria infection can grow to hypoglycemia, cerebral malaria or anemia as result the blood carrying capillaries are blocked due to the thickness of blood. This happens, when the parasite is drug resistant or there is a lack of availability in proper medicines. The cerebral malaria is a key factor of lifetime learning disabilities (11), it can cause coma and further may lead to death.

There have been few studies in the field of regional classification of malaria-proneness. Recently, Santosh *et al*. (12) presented an artificial neural network (ANN) that uses a sigmoid function as

an activation function in a prediction model for malaria using data engineering, for the southern regions of India, and addressed the problems of scalability and time complexity for traditional machine learning algorithms. For classification, a feedforward multilayer perceptron (MLP) is a widely used neuron model that uses backpropagation (BP) as a learning method with weight updating (13). Feedforward nets are efficient in terms of classification, but are time-consuming.

The first artificial neuron was proposed by McCulloch *et al.* (14), and was known as a linear threshold unit (LTU) or threshold logic unit (TLU). This model was a mathematical interpretation of a neuron. Sharp *et al.* (15) proposed an electrical model of an artificial neuron and explained the oscillation properties exhibited by this neuron. Izhikevich (16) introduced the concept of resonate and firing in neural activities, which exhibited biological properties. In recent years, spiking neuron models (third-generation ANNs) are used in classification and prediction problems and these have shown improvements over conventional neuron models. Abbott (17) introduced the concept of threshold values for spike generation, and stated that an integrate-and-fire neuron (IFN) exhibits almost all of the characteristics of pharmacological input neurons or natural neurons. Abbott *et al*. (18) developed a generalized non-linear IFN for electrical circuits. Stein *et al.* (19) developed a new model by introducing a leaky term into the IFN and it was added to the membrane potential, the model was termed a leaky IFN (LIFN), and this model was developed as a special case of the generalized IFM model. Nicolas *et al*. (20) proposed another special case called the quadratic IFN (QIFN), which was derived from the generalized IFN model. Fourcaud *et al*. (21) presented an exponential IFN (EIFN) neuron model which uses an input current in the form of an exponential or spiking current. A further description of spiking neural networks is presented in the Discussion section.

The interspike interval (ISI) is a key factor affecting the passing of information from one neuron to another. Yadav *et al.* (13) observed that ANNs are efficient in performing pattern classification when the biological properties of the neuron are included. The authors used an MLP with an ISI derived from IFN, and this yielded better accuracy and lower time complexity. We thus hypothesize that the ISI obtained from the proposed neuron model with a BPNN will yield a regional classifier for our objective solution. This neuron mimics the characteristics of natural neurons, and when embedded with BPNN, can provide a more robust solution. This study presents an ISI-based BPNN (ISI-BPNN) function in which the proposed architecture is a single-pass spiking learning strategy which is useful for nonlinear regression tasks.

Based on this approach, we implemented an architecture that leads to the following contributions: (i) the design of a new spiking function for a nonlinear IFN model (NLIFN) and its ISI; (ii) this ISI is then used as an aggregation function in a BNN, and is referred to as an ISI-BPNN. In addition, weight updating equations are derived and comparative studies are performed via experiment; (iii) real-world malaria data are used in a comparative performance evaluation of the proposed ISI-BPNN.

The rest of the paper is organized as follows: Section 3 presents a mathematical model of the spiking function along with the ISI-BPNN architecture. Machine learning architecture is discussed in Section 4, and the experimental protocol involving a real-world malaria dataset is discussed in Section 5. The results of experiments using the proposed method are presented in Section 6. A performance evaluation of ISI-BPNN is conducted in Section 7, and Section 8 contains a scientific validation and statistical analysis. In Section 9, we summarize the paper and present a discussion of the proposed design, including benchmarking, special notes on the sigmoid function and neural networks and their strengths and weaknesses, and future work. Finally, the study is concluded in Section 10.

3. DERIVATION OF THE PROPOSED MODEL

A spiking neuron model closely mimics and simulates the computational characteristics of a natural neuron. The IFN was the first model of a biological neuron, and was designed using a simple R-C circuit (11). In an IFN, action potentials are represented as an event, often termed a spike, and

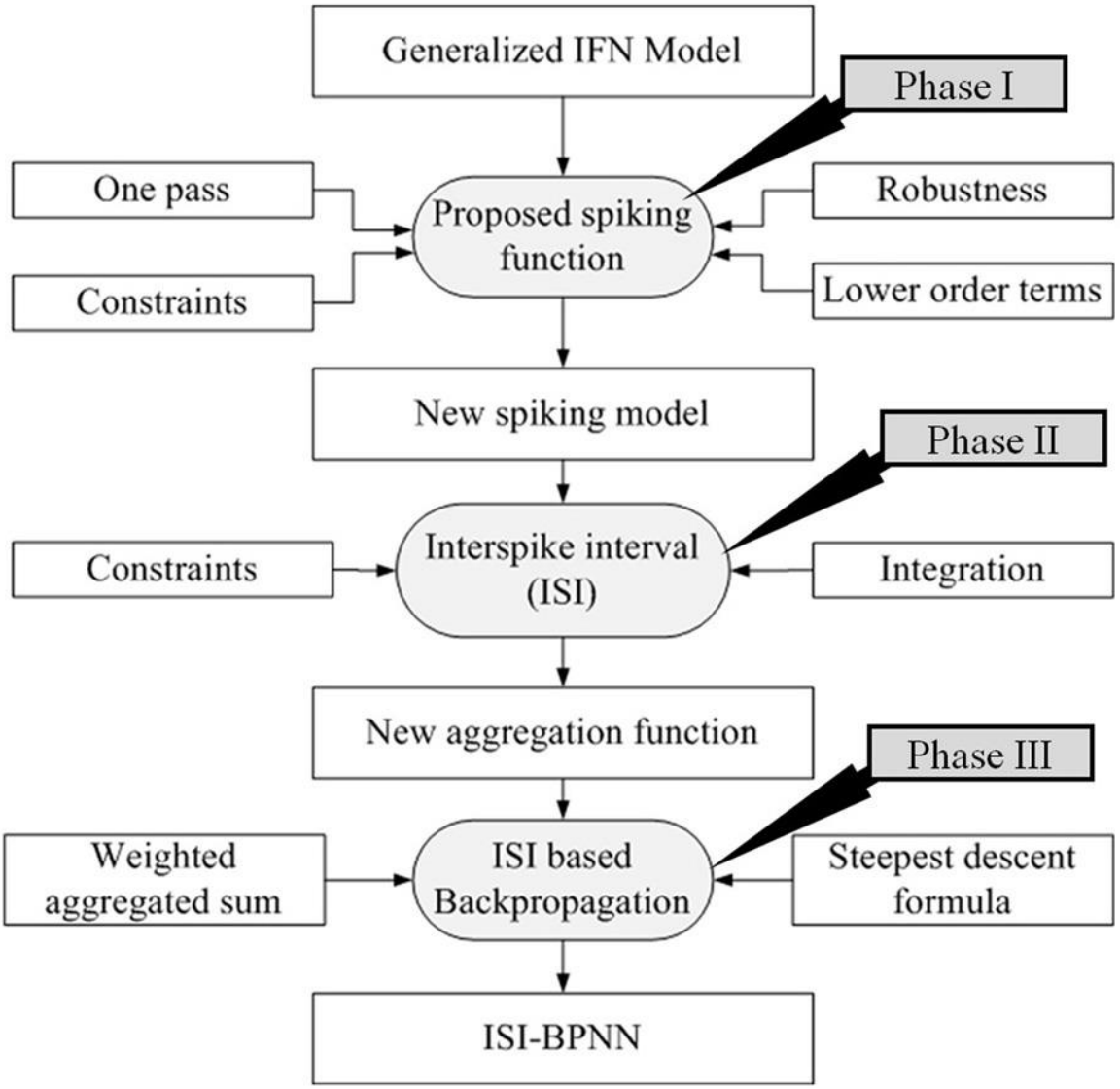

Figure 2. Object process model showing the aggregate sum used in the design of ISI-BPNN

neurons communicate with each other based on spike time intervals.

3.1. Proposed system

The design of the proposed system is inspired by the generalized IFN model. We create a spiking function, and the aggregated output is used as input to the sigmoid function in the BP algorithm. We therefore call our approach ISI-BPNN. The global model is shown in Figure 2. The object process diagram illustrates the procedure of the model development, and contains three processes: the design of the spiking function, the design of the ISI and the integration of ISI with BPNN, as shown by three different ellipses. The spiking model (phase I) is designed using the generalized IFN model, retaining features such as robustness, constraints and a single-pass model (derived in the next section). Phase II uses constraints and an integration model to generate the aggregate function. Phase III uses this weighted aggregated sum to generate the ISI-BPNN,

using the steepest descent paradigm. Following this, the input to the sigmoid function is constructed, and finally, the new classifier is obtained from the sigmoid function.

3.2. Nonlinear integrate-and-fire neuron model

An IFN is an efficient model that is capable of computing the characteristics of a biological neuron over time. In an IFN, the membrane potential is directly proportional to an externally injected current. When this current is injected, the voltage potential rises, and after a certain time settles down to a threshold value. Once the membrane potential reaches a desired threshold, it generates a spike and then resets the voltage immediately after this spike. Usually, a biological neuron has memory, an equivalence term called a leak term is added to an IFN, and this is known as an LIFN. This is the most representative model of an actual biological neuron. The memory term is included in an action potential that represents the diffusion of ions inside the membrane cell. Biologically, diffusion occurs when the membrane cell is in disequilibrium. The generalized nonlinear IFN (21) is represented as:

$$\tau \frac{dV}{dt} = -g_L\left(V - V_L\right) + L(V) + M(V)I_{ext} \quad (1)$$

where τ is the membrane constant, V is the membrane potential at time t, g_L is the leaky inductance of the membrane, I_{ext} represents the external input current, and $L(V)$ and $M(V)$ represent the generalized functions of the membrane potential. We can obtain the QIFN by substituting a specific function of second order (V^2) for the membrane potential (V) and can obtain the EIFN model by substituting an exponent term ($\exp(V)$ or $e^{(V)}$) as a specific function for the membrane potential in the general equation for a nonlinear IFN, as shown in Eq. (1).

3.3. Proposed spiking model

A new spiking model for a nonlinear IFN is proposed in this work. The proposed spiking function has the form, $L(V) = \frac{a}{V} - \left(\frac{b(V - V_t)}{1 + (V - V_t)^2}\right)$ where a and b are positive numerals and have the relation: $a = \frac{g_L V_t^3}{2\Delta_t}; b = g_L\left(1 + \frac{V_t}{2\Delta_{tt}}\right)$, V represents the membrane potential, V_t and V_t^3 represent the membrane potential function at time t and the cubic power function of V_t respectively and g_L is the inductance of the membrane. If we substitute the values of $L(V) = \frac{a}{V} - \left(\frac{b(V - V_t)}{1 + (V - V_t)^2}\right)$ and $M(V) = R$ into Eq. (1), i.e. $\tau \frac{dV}{dt} = -g_L\left(V - V_L\right) + L(V) + M(V)I_{ext}$ and the values of a and b are substituted, we obtain an updated equation as given in Eq. (2):

$$\tau \frac{dV}{dt} = -g_L\left(V - V_L\right) + \frac{g_L V_t^3}{2V\Delta_t} - \frac{g_L}{2\Delta_t}\left(\frac{(2\Delta_t + V_t)(V - V_t)}{1 + (V - V_t)^2}\right) + RI_{ext} \quad (2)$$

where, V, V_L, I, t, τ and Δ_t are the membrane potential, leak potential, external current input, time, membrane time constant, and incremental time, respectively (the derivation of Eq. (2) is given in the Supplementary Material). Once the potential V reaches a threshold voltage V_{thres}, the membrane potential dynamics are interspersed, and then the potential is then reset after the spike following re-initialization at a resting potential of V_{rest}. The term $L(V)$ is obtained by comparing the RHS of Eq. (1) and Eq. (2). The response from the firing rate of the proposed neuron model is analytically calculated as the first derivative of $L(V)$, i.e.

$$L'(V) = \frac{g_L}{V_t^2}\left(\frac{V_t^3}{2\Delta_t}\right) + g_L\left(1 + \left(\frac{V_t}{2\Delta_t}\right)\right)\left\{\frac{1 - (V - V_t)^2}{\left(1 + (V - V_t)^2\right)^2}\right\} \quad (3)$$

It is observed that the derivative $L^{'}(V)$ satisfies the properties of nonlinear neuron model, i.e.

$$L^{'}(V_T) = g_L \tag{4}$$

Furthermore, this nonlinear model also meets the requirements of the condition of the spike sloping factor (Δ_t), i.e.

$$L^{''}(V_T) = \frac{g_L}{\Delta_t} \tag{5}$$

The proposed function has a lower order than the other spiking functions including $\exp(V)$, V^2 and V proposed earlier. Biologically plausible spikes are generated by this proposed function. The LHS of Eq. (1) can be denoted by $F(V,I)$, a nonlinear potential of the membrane, and this is given as:

$$F(V,I) = \frac{a}{V} + b*\left(\frac{V}{1+V^2}\right) + R.I_{ext} + c \tag{6}$$

where, $a = \frac{g_L V_t^3}{2\Delta_t}$; $b = g_L\left(1+\frac{V_t}{2\Delta_t}\right)$ *and* c is a constant; * is the multiplier; R is the resistance of the membrane; and I_{ext} is the external input current (and thus the product of the latter two parameters represents the voltage). The spikes obtained using a two-dimensional function $F(V,I)$ from Eq. (2), at $I = 10A$ are shown in Figure 3(b). Izhikevich (23) stated that function $F(V,I)$ should satisfy non-degeneracy and transversality conditions. Eq. (5) shows that a partial derivative of $F(V,I)$ with respect to I is not equal to zero. Hence, $F(V,I)$ also satisfies the property of transversality and $F(V,I)$ satisfies the property of non-degeneracy, since the second derivative is not equal to zero.

3.4. Interspike interval and firing rate of the proposed spiking model

The ISI is the main source of information exchange, and appears in mammalian neurons (19). The zero-order solution of Eq. (2) gives an ISI that is responsible for inter-neuron communication. The ISI in the proposed model is given by Eq. (7) as follows:

$$t_{ISI} = \frac{1}{2\tau(a+b^3)}\left(\frac{\gamma * \tan^{-1}(\alpha)}{\sqrt{\beta}} + \beta_1 - \beta_2\right) + c \tag{7}$$

where

$$\begin{cases} \alpha = \dfrac{2a(V-V_t)+b(V_t-2V)}{\sqrt{4a^2+4ab-b^2V_t^2}} \\ \beta = 4a^2+4ab-b^2V_t^2 \\ \beta_1 = b\{a(1-c^2)+b\}\log\{(a+b)(V-V_t)\} \\ \beta_2 = (a+b)(V-V_t)\{(a+b)(V-V_t)-2ac\} \\ \gamma = 2V_t b\left(4a^2+ab\left(V_t^2+5\right)+b^2\right) \\ c \text{ is a constant} \end{cases}$$

The firing rate or frequency (ϕ) is the inverse of time, and thus $\phi = t_{ISI}^{-1}$:

$$\phi = \frac{1}{\frac{1}{2\tau(a+b^3)}\left(\frac{\gamma * \tan^{-1}(\alpha)}{\sqrt{\beta}} + \beta_1 - \beta_2\right) + c} \tag{8}$$

The spike generation timing is also known as the ISI, as shown in Eq. (7), and is necessary for the biological neurons to communicate. The integrated solution is given in Eq. (7) and is used in the construction of the aggregation function, which is also used as an activation function in the ISI-BPNN. The firing pattern exhibited by the model is shown in Figure 3. We can see from Figure 3(a) and Figure 3(b) that the spikes generated by IFN and ISI-BPNN are similar. The key benefit of the proposed spike-

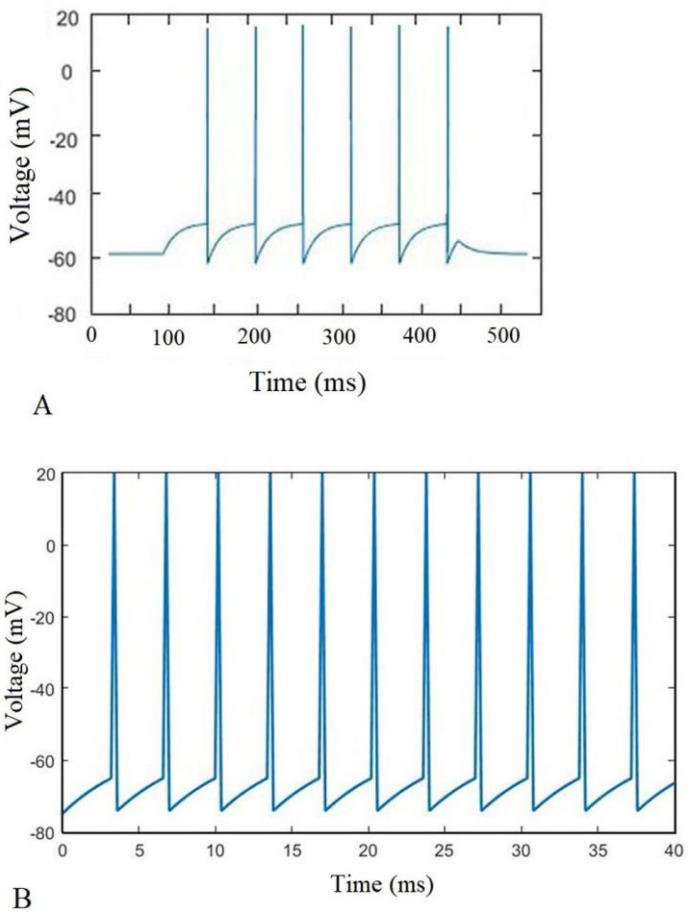

Figure 3. Spike dynamics (a) IFN, (b) ISI-BPNN

generating function is that it contains lower-order terms than other existing quadratic and exponential neuron models. The spike-generating function also reduces the computational complexity.

3.5. Construction of a new aggregation function

The new aggregation function for ISI-BPNN is derived from Eq. (2), as explained in this section. A parametric representation of Eq. (7) can be given as:

$$T_{ISI} = P*\left(A*tan^{-1}(Bx+C)+D*\log(Ex+F)+Gx^2+Hx+Z\right) \quad (9)$$

where,

$$A=\frac{2V_t b\left(4a^2+ab\left(V_t^2+5\right)+b^2\right)}{\sqrt{4a^2+4ab-b^2V_t^2}}$$

$$B=\frac{2(a-b)}{\sqrt{4a^2+4ab-b^2V_t^2}}$$

$$C=\frac{-V_t(a+b)}{\sqrt{4a^2+4ab-b^2V_t^2}}$$

$$D=b\left(a\left(1-V_t^2\right)+b\right)$$

$$E=a+b$$

$$F=-V_t(a+b)$$

$$G=(a+b)^2$$

$$H=-2(a+b)^2V_t-(a+b)V_t$$

$$P=\left(\frac{1}{2\tau(a+b^3)}\right)$$

$$Q=V_t^2\left((a+b)^2-2aV_t(a+b)\right)$$

The variable voltage V is replaced by x

T_{ISI} represents the Interspike Interval

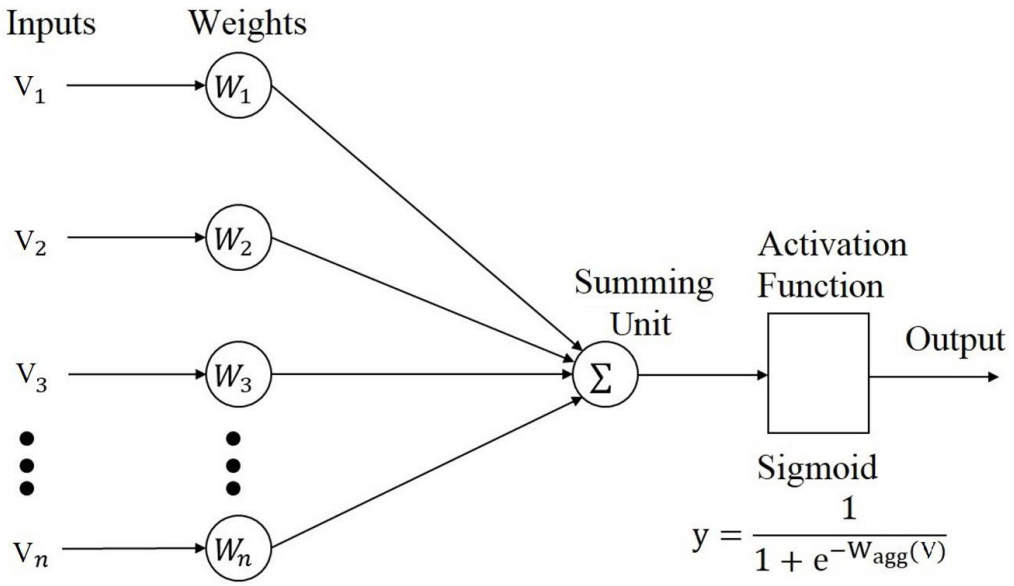

Figure 4. Computation of the aggregated weight function

The computation of the new ISI-based BNN is shown in Figure 4. The network diagram consists of two layers. Input V has K attributes, and the first layer has neurons for each distinct feature and the second layer is the output layer.

Assuming that the input to the j^{th} neuron is V_j and that the corresponding weights are $a_j, b_j, c_j, d_j, f_j, g_j, h_j, p_j, q_j$, and that K input neurons $(V_1, V_2 \ldots, V_K)$ are connected to the m^{th} neuron in the second layer, then the weighted aggregate $W_{agg}(V)$ at m^{th} neuron is defined as:

$$W_{agg}(V) = \sum_{j=0}^{K}\left[a_j * tan^{-1}(b_j V_j + c_j) + d_j \log(f_j V_j + g_j) + h_j V_{j^2} + p_j V_j + q_j\right] \quad (10)$$

where K is the number of input neurons.

3.6. Proposed ISI-BPNN and training algorithm

This subsection explains the development of ISI-BPNN and the training algorithm used. After the construction of the proposed network is explained, the training algorithm is given based on the steepest-descent formulae.

3.6.1. Construction of the proposed isi-based backpropagation (ISI-BP)

In the creation of the proposed network, W_{agg} is treated as the input for the activation function and is considered to be analogous to the input to the neuron and the ISI. Hence, it can be assumed to be a function of the externally injected current I_{ext}. Weights are associated with the corresponding inputs for the temporal summation when other synapse inputs are present. The other part of the IFN is represented in terms of a threshold function. Here, to represent the activity of this block, a sigmoid function is used in which the aggregated function $W_{agg}(V)$ is used instead of x. Thus, the sigmoid function is written as in Eq. (11):

$$y = \frac{1}{1 + e^{-W_{agg}(V)}} \quad (11)$$

where, y is an s-shaped sigmoid function that lies between zero and one, meaning that when

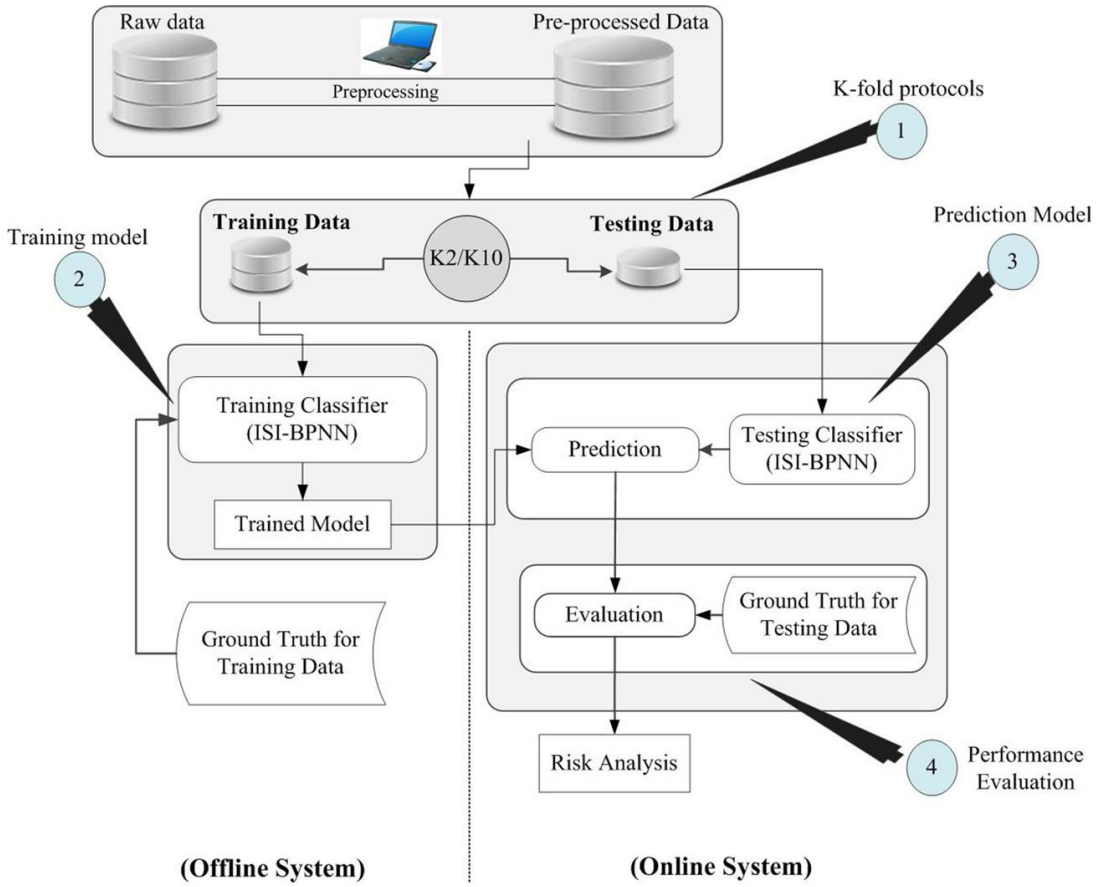

Figure 5. Machine learning architecture

the input tends to infinity, this function achieves its highest value of one, and when the input tends to negative infinity, it achieves its lowest value of zero.

4. MACHINE LEARNING ARCHITECTURE

The machine learning architecture for the proposed scheme is given in Figure 5, which illustrates the entire process from the very beginning, including data collection, to the evaluation and validation of the model. In the first step, the collected data were preprocessed and a dataset prepared for classification. The K2 and K10 protocols were then applied to the dataset to prepare the training and testing data. The training data were used in classifier training, which generates the training coefficients. These coefficients were then used to transform the test dataset to compute the predicted classes of malaria-prone regions, that is, high or low risk. This process was repeated for the K2 and K10 protocols and the MLP, SVM, IFN, GCNN classifiers. Cross-validation was used to compute the accuracy of the machine learning architecture. The results of the prediction were validated to ensure the robustness of the system.

4.1. Conventional classifiers

The developed model was tested against conventional classifiers such as MLP, IFN, SVM, and GCNN. The theoretical concepts underlying these classifiers are discussed in this section.

4.1.1. Multilayer perceptron

The MLP is a feedforward artificial neural network (36) with a minimum of three layers: the first is an input layer, the second a hidden layer and last an output layer. The activation function is used at

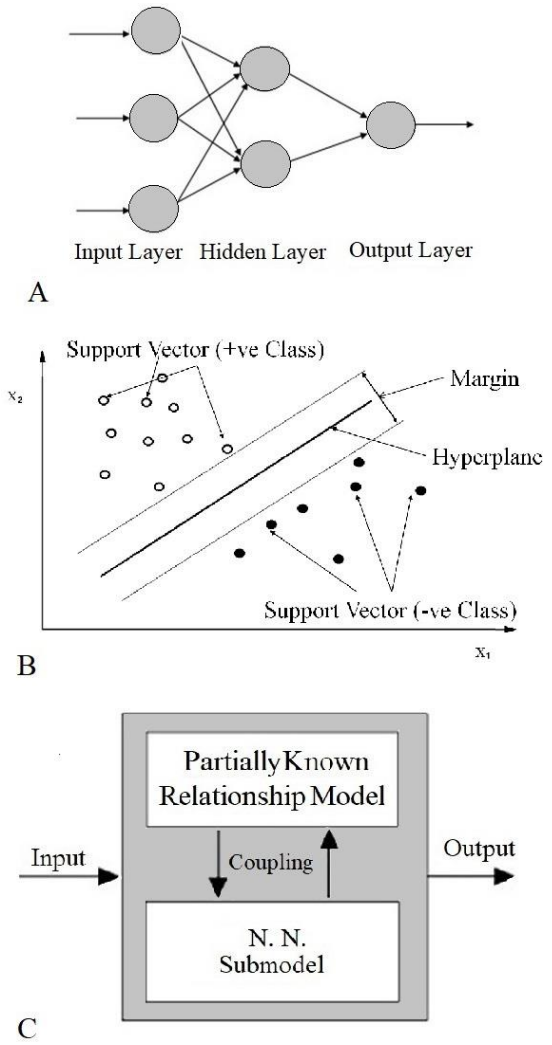

Figure 6. Conventional classifiers (a) MLP, (b) SVM and (c) GCNN

each layer in the MLP except the input layer. Figure 6(a) shows the traditional model of a feedforward network.

4.1.2. Support Vector machine

Support vector machines (SVMs) (37) are supervised classifiers that are used in classification and regression tasks. An SVM has a separating hyperplane by which it classifies the data. It is the most suitable model for labeled data classification, and uses a representation of points in a hyperplane that are categorized in terms of a positive or negative class. It uses a certain margin, based on which the labels are categorized as shown in Figure 6(b).

4.1.3. Generalized-constraint neural network

A generalized-constraint neural network (GCNN) (38) consists of three units: an input, a processing unit, and an output unit. The processing unit contains two subunits: a neural network sub-model and a partially known relationship model. During execution, there is a coupling between the units that allows the system to classify the input data when partially known relationships are applied to the input. The model is shown in Figure 6(c), which explains the conceptual working of GCNN.

5. DATA COLLECTION AND EXPERIMENTAL PROTOCOL

This section presents the details of the data collection and the experiments performed. The proposed ISI-BPNN model is applied to a real-time dataset of malaria disease. Throughout the work, in terms of achieving the goal, experimental paradigms are used. We develop the ISI from the proposed function, develop an aggregation function, and finally develop the ISI-BP model and obtain its learning rule based on the aggregated function. We compute cross-validation protocols to examine the quality with regard to the generalized datasets for each approach. The first experiment is performed to test the effect on accuracy by making changes in the size of training data, using two methods of K-fold validation (K2 and K10). In the second experiment, we increase the size of the dataset and then apply K-fold techniques. The model is also tested for accuracy.

5.1. Data collection

The malaria data used in this study were collected from a government infectious disease (ID) hospital in Ponda, Goa, via a Department of Science and Technology (DST), Science and Engineering Research Board (SERB) project at the National Institute of Technology Goa, India.

5.1.1. Demographics, recording protocol and ground truth

The data was collected over a three-year period from January 2015 to December 2017. Four attributes were measured: temperature, humidity,

rainfall and the number of patients taken from 43 villages. The cohort consisted of 2,210 females and 2,564 males. Each record consisted of three attributes: temperature, humidity and rainfall. In all, 4,744 records were collected over this period, and the distribution was as follows: for the first month, three attributes (temperature, humidity and rainfall) were recorded for 43 villages, giving 43x3=129 records. In the first six months, 43x3x6=774 records were taken; over the first year, the total records were: 43x3x12=1548; and over the entire three-year period, the total number of records was: 43x3x12x3=4,744. Patients were recorded as testing positive or negative for malaria based on blood sample examinations. All the recordings were done in the register by hospital nurses. Positive malaria cases were recorded as a value of 1 (with malaria) and blank columns were treated as a value of 0 (no malaria). These binary data formed the ground truth information for the study. The collected malaria data contained records on patient visits, residential location and gender information.

5.1.2. Meteorological data

The dataset consisted of the metrological attributes of temperature, rainfall and humidity as input, and the number of patients from a specific location as the target values. Attribute values were as follows: Average temperature (month high (°C)/low (°C)): Jan 32/20, Feb 32/21, Mar 33/23, Apr 33/25, May 34/26, Jun 31/25, Jul 29/24, Aug 29/24, Sep 30/24, Oct 32/24, Nov 33/22, Dec 33/21. Relative humidity (month humidity (%)): Jan 63%, Feb 64%, Mar 65%, Apr 67%, May 69%, Jun 84%, Jul 87%, Aug 88%, Sep 85%, Oct 78%, Nov 68%, Dec 62%. Average rainfall (month rainfall (mm)): Jan 0, Feb 0, Mar 2.54, Apr 17.78, May 104.14, Jun 678.18, Jul 985.52, Aug 589.28, Sep 231.14, Oct 132.08, Nov 35.56, Dec 12.7.

5.1.3. Geographical location of villages

The geographic locations of villages in the Ponda area are shown on the map of Goa (the study area is shown in the Supplementary Material). The dataset consisted of records of patients from 43 villages around Ponda, as follows: 1. Adcolna, 2. Adpai, 3. Bandora, 4. Betora, 5. Boma, 6. Borim, 7. Candepar, 8. Candola, 9. Codar, 10. 11. Conxem, 12. Cuncoliem, 13. Cundaim, 14. Curti, 15. Dhavali, 16. Durbhat, 17. Farmagudi, 18. Gangem, 19. Jay Cee Nagar, 20. Kaziwada, 21. Keri, 22. Khadpabandh, 23. Marcaim, 24. Nageshi, 25. Nirancal, 26. Orgao, 27. Ponchavadi, 28. Priol, 29. Quela, 30. Querim, 31. Sadar, 32. Sahapur, 33. Santa Cruz, 34. Shanti Nagar, 35. Siroda, 36. Telaulim, 37. Tisk, 38. Tivrem, 39. Undir, 40. Usgao, 41. Vagurbem, 42. Velinga, 43. Volvoi.

5.1.4. Ethics approval

The collected malaria data were given ethical approval from the Infectious Disease Hospital, Ponda, Goa, India. The patient records were maintained manually in the registers and these records were then converted into computerized datasheets by the hospital before being transferred for this study. During the study, double checking for errors was carried out after the data had been transferred from the hospital to Institute. During computerization, the patient records were anonymized.

5.2. Experiment 1: Computation of accuracy of ISI-BPNN using K2 and K10 cross-validation

The motive for performing this experiment was to examine the effects of changes in accuracy by making changes in the training set using the K2 and K10 protocols. Each fold is a subset of our dataset; K2 means that the data were divided in to two parts in a 1:1 ratio, i.e. half (50%) for training and half (50%) for testing, whereas K10 means that the data were divided into 10 parts in a 9:1 ratio, meaning that 90% of data were used for training and 10% for testing. These experiments were repeated 10 times on a random basis, and the average accuracy was recorded.

5.3. Experiment 2: Effect of Training Set Using ISI-BPNN for Datasets

The motive for this experiment was to identify changes in performance by making changes to the dataset sample size. The sample size played a vital role in both performance and computation time during every iteration. We used four sizes of datasets: monthly, half-yearly, yearly and combined three-year data, and these were termed CN1, CN2,

CN3 and CN4 which contains 129, 774 , 1548 and 4744 records respectively. It was therefore necessary to run K-fold protocols for these four types of datasets.

5.4. Experiment 3: Inter-Classifier Comparison

The aim of this experiment was to perform a comparative analysis of ISI-BPNN and calculate the mean accuracies for other classifiers including SVM, IFN, GSNN and MLP.

6. RESULTS

This section presents the experimental results, and is divided into three subsections. In the first subsection, the results of Experiment 1 are presented and a comparative analysis is carried out; in the second subsection, the results obtained in Experiment 2 are presented; and in the third subsection, the results of Experiment 3 are given in detail. Symbols used in this paper are listed in Table 2.

6.1. Results of experiment 1

The system accuracy (η_{sys}) can be expressed using the following function:

$$\eta_{sys}(k) = \frac{\sum_{t=1}^{T}\sum_{l=1}^{N_m}\eta(k,l,j)}{T * N_m} \quad (12)$$

where, k is the partition protocol i.e. K2 or K10. T, t, l, N_m are the number of trials, the index of the trial number, the dataset index and the size of the data respectively, as shown in Figure 7, in the figure, numbers on the bar are standard deviation. The accuracies for the K2 and K10 protocols are represented in green and purple, respectively. As can be seen from the figure, the proposed ISI-BPNN scheme exhibited an average accuracy for K2 and K10 of **91.78%** and **98.06%,** respectively. Figure 8, Figure 9 and Figure 10 show the monthly prediction results of our proposed algorithm for the years 2014, 2015 and 2016 respectively. We can observe from these Figures that our proposed algorithm gives the desired results, as the predictions are much closer to the actual cases. Here, we can clearly observe that for consecutive years, our model gave very accurate predictions and performed well, requiring less computational time.

6.2. Results of experiment 2

To identify the effects of the size of the training data on the ISI-BPNN and other classifiers, we carried out an experiment by varying the size of the dataset. We conducted experiments on datasets of different sizes, i.e. CN1, CN2, CN3 and CN4. The accuracies for the K10 protocol obtained from these varying data are shown in Figure 11 (a) and the corresponding data are given in Table 3 where we can conclude that as the size of the dataset increased, the model became well-trained, and outperformed the other methods by yielding accuracies of **98.67%** for DC3 and **99.28%** for the DC4 dataset.

6.3. Results of experiment 3

The results for different classifiers are shown in Figure 11 (b), and the corresponding data are given in Table 3. The SVM, IFN, MLP, GCNN, and ISI-BPNN classifiers exhibited average accuracies of 85.14%, 89.8%, 87.6%, 87.0% and 91.78%, respectively, for the K2 protocol. Prediction results for the K2 and K10 protocols are listed in Table 4 respectively. In Table 5, the average improvement in accuracy for the K2 and K10 protocols is compared with the ISI-BPNN scheme; the ISI-BPNN model exhibited an 11.9% increase in accuracy over the conventional classifiers.

7. PERFORMANCE EVALUATION

Any modeling procedure needs to be subjected to testing, verification and validation. These procedures are used to determine an accurate fit of the model to the phenomenon being modeled. Regardless of which modeling procedure is followed, the performance of the model shows the first insight of representation as expected for a real-time scenario in systems.

Table 2. Symbols used and their description

SN	Symbols	Description of Symbol
1	a_i	Constant associated with aggregated function
2	b_i	Constant associated with aggregated function
3	c_i	Constant associated with aggregated function
4	d_i	Constant associated with aggregated function
5	f_i	Constant associated with aggregated function
6	g_i	Constant associated with aggregated function
7	h_i	Constant associated with aggregated function
8	p_i	Constant associated with aggregated function
9	q_i	Constant associated with aggregated function
10	A	Derived intermediate variables
11	B	Derived intermediate variables
12	C	Derived intermediate variables
13	D	Derived intermediate variables
14	F	Derived intermediate variables
15	G	Derived intermediate variables
16	H	Derived intermediate variables
17	P	Derived intermediate variables
18	Q	Derived intermediate variables
19	α	Derived intermediate variables
20	β	Derived intermediate variables
21	β_1	Derived intermediate variables
22	β_2	Derived intermediate variables
23	γ	Derived intermediate variables
24	y	Obtained value

contd...

Table 2. Contd...

SN	Symbols	Description of Symbol
25	t	Target value
26	e	Error
27	T_{ISI}	Interspike timing
28	V	Membrane potential
29	V_L	Leak potential
30	V_{thres}	Threshold potential
30	I_{ext}	External current
31	g_L	Leak conductance of the membrane
32	Δ_t	Fractional time
33	W_{agg}	Aggregated weight
34	τ	Membrane constant
35	η(k, l, t)	Accuracy for k^{th} protocol, I^{th} , and t^{th} trial
36	η_{sys}	System accuracy
37	N_m	Total size of malaria dataset
38	T	Total number of trials
39	old	Previous value
40	new	Updated value
41	ψ	Learning factor
42	Φ	Frequency
43	K	Number of inputs
44	E_{seg}	Exposure index of segregation
45	I_{seg}	Isolation index of segregation
46	D_d	Dissimilarity index
47	X	Total number of patients

contd...

Table 2. Contd...

SN	Symbols	Description of Symbol
48	Y	Number of malaria positive cases
49	N	Population
50	D_E	Exposed diseased
51	H_E	Exposed healthy
52	D_N	Non exposed diseased
53	H_N	Non exposed healthy
54	T_{max}	Maximum temperature
55	T_{min}	Minimum temperature
56	Prm	Parameter
57	c	Arbitrary constant
58	CL	Classifier
59	WN	Week number
60	SD	Standard deviation
61	SN	Serial number

The performance of the model can be assessed based on very different aspects. The primary purpose of the verification process is to confirm whether or not the desired output is obtained. The quality of the model is always a critical issue (24), and this study therefore implements a two-phase performance evaluation to ensure both the reliability and the stability of the system.

7.1. The Receiver operating characteristic curve

The receiver operating characteristic (ROC) curve is used to validate the diagnostic capability of the ISI-BPNN classifier. The plotted curve and corresponding area under the curve (AUC) is shown in Figure 12. The AUC is **0.9636** for ISI-BPNN, implying a 96% chance (or probability of 0.96) that model classifies the data correctly. Thus, the system is accurate enough to perform binary classification. Conventional classifiers have a lower AUC(s).

7.2. Sensitivity analysis

In the sample dataset, as shown in Table 6, there are four features to be input to the system and one response variable. The ground truth variables are the maximum and minimum temperatures, rainfall, and humidity. The threshold for maximum temperature is 40 ± 2.5°C, for minimum temperature 15 ± 2.5°C, for rainfall 120 ± 5 mm and for humidity 40 ± 5%. The accuracies are recorded in order to analyze the sensitivity to the variables, and are shown in Figure 13, Figure 14, Figure 15, and Figure 16, for the four variables. It is clear from the standard deviation shown in Table 7 that the model has low sensitivity (< 5%) to all parameters. Other classifiers also have low sensitivity; however, ISI-BPNN is more robust than IFN, MLP, SVM and GCNN.

8. SCIENTIFIC VALIDATION

Validation defines the stability and robustness of the system. In this study, the

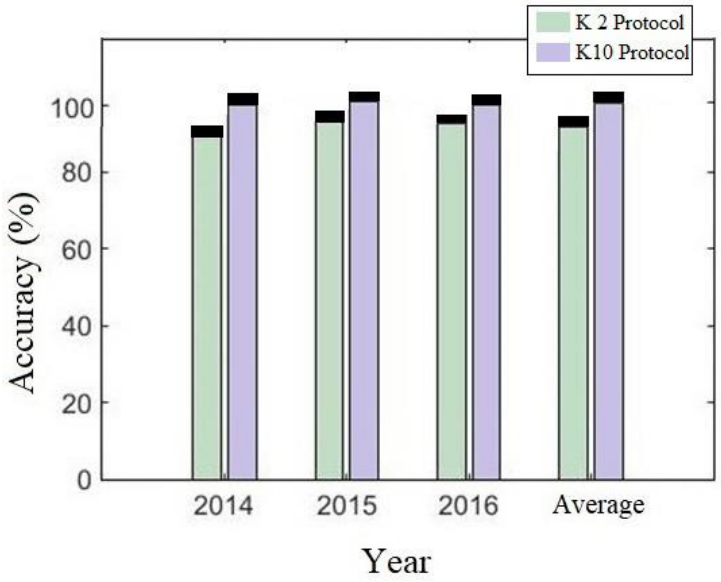

Figure 7. Prediction results of ISI-BPNN for K-fold protocols (numbers on the bar are standard deviation)

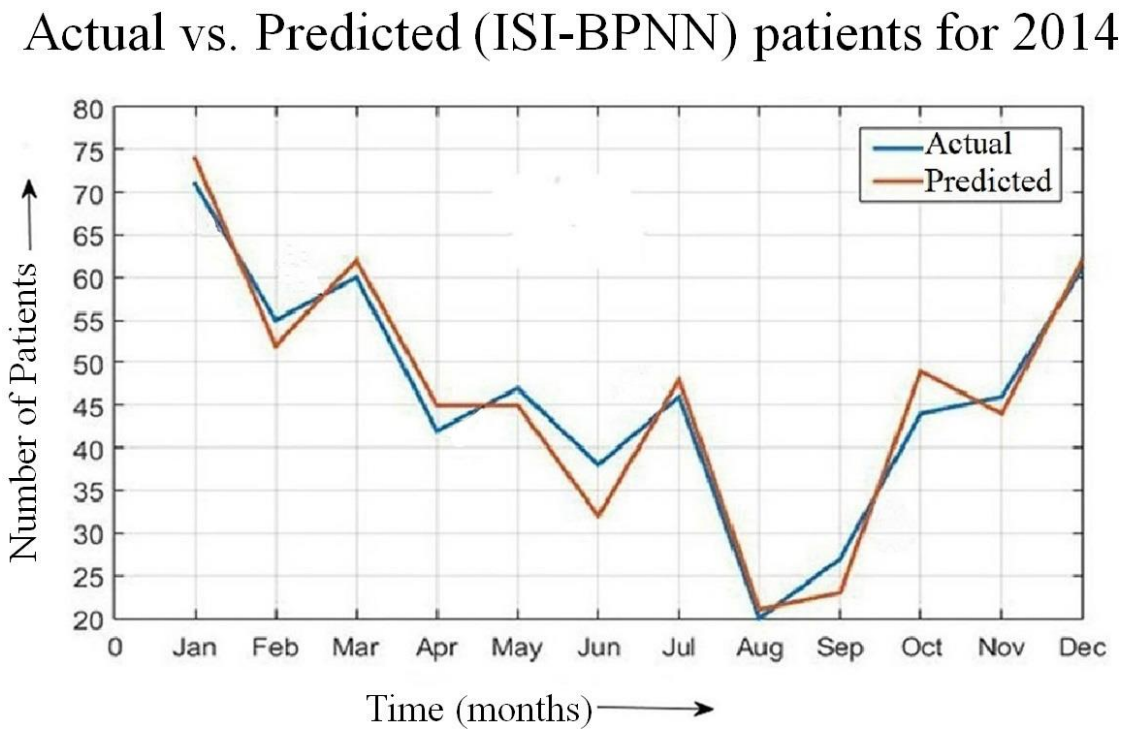

Figure 8. Actual vs. predicted malaria patients for the year 2014

aggregated function can control the system dynamics. To validate the ISI-BPNN, two synthetic datasets are used and the malaria segregation index is calculated. In order to validate the proposed model, we use two datasets from the UCI machine learning repository called Thoraric Surgery

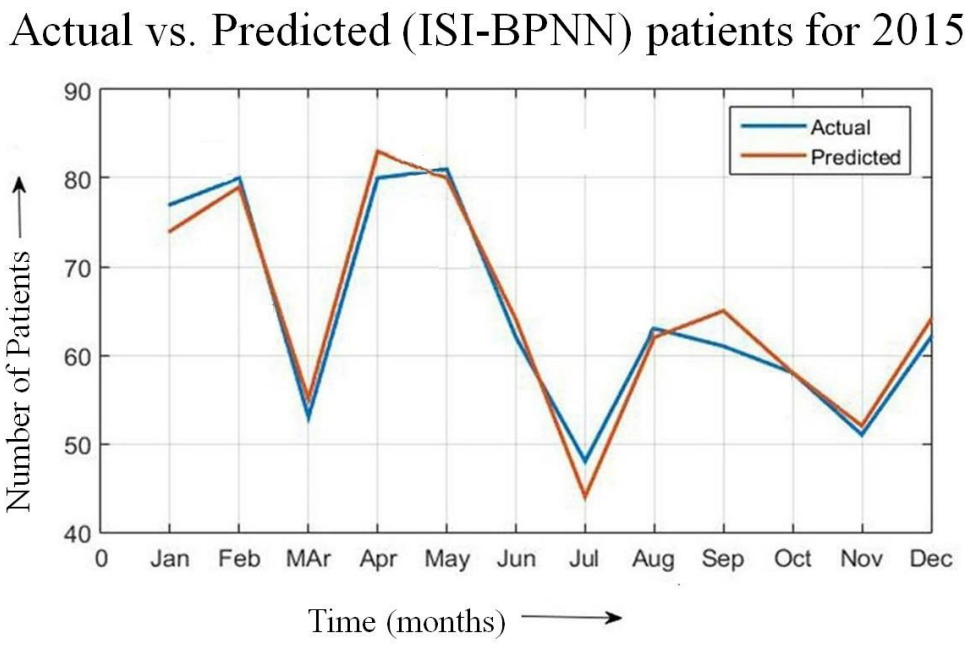

Figure 9. Actual vs. predicted malaria patients for the year 2015

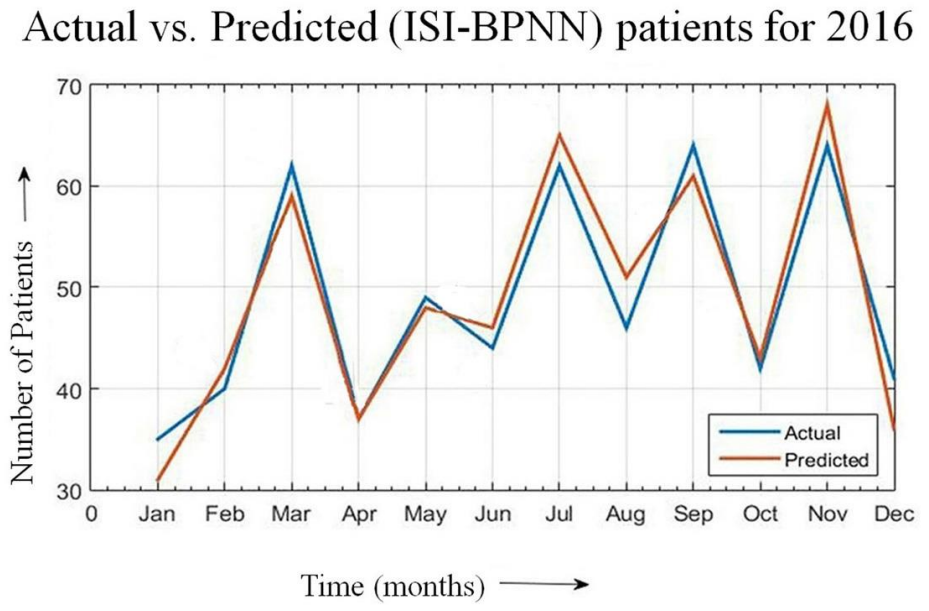

Figure 10. Actual vs. predicted malaria patients for the year 2016

(https://archive.ics.uci.edu/ml/datasets/Thoracic+Surgery+Data#) and Parkinson's Disease (https://archive.ics.uci.edu/ml/datasets/parkinsons). The UCI repository has the largest available collection of datasets for performing tests on machine learning and artificial intelligence. The Thoracic

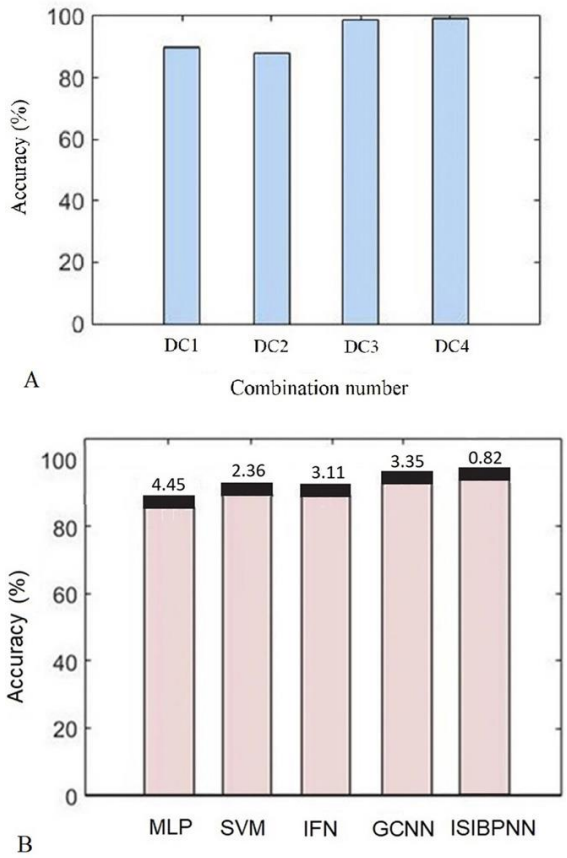

Figure 11. Prediction accuracies for (a) different data sizes (b) different classifiers (numbers on the bar are standard deviation)

Surgery dataset has 17 attributes and 470 instances associated with classification problems. It has two classes, true (Y) and false (N), and of the 470 records, 70 are true instances and 400 false**.**

8.1. Malaria segregation index (MSI)

Segregation analysis is performed in order to statistically validate the developed model. The index of dissimilarity, segregation, exposures and odds ratio/ risk ratio are calculated. These as given as follows:

8.1.1. Index of Dissimilarity

To find the dissimilarity, we need to calculate the distribution of malaria and non-malaria throughout the evaluations of a particular village. The index has a minimum value of zero and a maximum of 100.

$$Dissimilarity(D_d) = \frac{1}{2}\sum_{i=1}^{N}\left|\left(\frac{X_i}{X} - \frac{Y_i}{Y}\right)\right| \quad (13)$$

where X_i, Y_i, X, Y and N are the number of cases in a particular village, the non-malaria cases in that village, total number of malaria patients throughout the year, total number of non-malaria cases throughout the year and the number of villages considered, respectively. The summation is applied to the total number of villages and the respective numbers of cases in that location. The average dissimilarity index for the nine villages in the Ponda area was **5.670.** Using a normalization scale of between zero and one, the DI is **0.0567.** The similarity can be computed as $S(\%) = (1 - D_d) * 100$, giving a percentage

Table 3. ISI-BPNN accuracies (%) in different data combinations

CN	ISI-BPNN
CN1	89.93
CN2	88.09
CN3	98.67
CN4	99.28
Average	93.99
SD	5.8

similarity of **94.3%.** From the above analysis, we conclude that ISI-BPNN is statistically significant, validating our hypothesis.

8.1.2. Isolation Index of segregation

The isolation index of segregation is given by:

$$I_{seg} = \sum_{v=1}^{N}\left(\frac{X_v}{X} * \frac{X_v}{N_v}\right) \quad (14)$$

where I_{seg} is the isolation index of segregation, and N_v is the total population of the v^{th} village. The isolation index obtained for the villages was very close to zero, meaning that the predictions made by ISI-BPNN were very close to the actual results. The isolation index obtained was 0.0011, implying that the majority (malaria) population and minority (non-malaria) populations are equally distributed among the villages.

8.1.3. Exposure or interaction measure of segregation

The exposure index of segregation is given by:

$$E_{seg} = \sum_{v=1}^{N}\left(\frac{X_v}{X} * \frac{Y_v}{N_v}\right) \quad (15)$$

where E_{seg} is the exposure measure of segregation, N_v is the total population of the village, Y_v is the number of non-malaria cases in that village and N is the number of villages. A lower exposure index means a lower dissimilarity between the predicted and actual results. All values are calculated based on the predicted number of cases with respect to the total population. The exposure index obtained for Ponda was **0.0149**, meaning that ISI-BPNN exhibited a very low dissimilarity between the actual and predicted results.

8.1.4. Odds ratio and risk ratio analysis

Odds ratios are the measure of the outcome and exposure of the disease. This measure is used to compute the stability of a system. If the odds ratio (OR) is equivalent to the risk ratio (RR), then system is considered to be stable. The values of exposed/non-exposed vs. diseased/healthy populations used to calculate the OR and RR are given in Table 8. The risk ratio and odds ratio are calculated as $RR = D_E * \left(\frac{N_N}{D_N * N_E}\right)$ and $\mathrm{OR} = D_E * \left(\frac{H_N}{D_N * H_E}\right)$, where D_E is exposed diseased, D_N is non-exposed diseased, H_E is exposed healthy, H_N non-exposed healthy, OR is the odds ratio and RR is the risk ratio, we have:

$$D_E = 2806, H_E = 57944, D_N = 47, H_N = 105033$$

$$N_E = D_E + H_E = 60750$$

$$N_N = 105080$$

Table 4. Classifier accuracies (%) in different data combinations in K2 protocol

K2 Protocol					
CN	MLP	SVM	IFN	GCNN	ISI-BPNN
1	86.45	86.31	80.27	85.81	92.58
2	87.34	82.35	86.45	85.68	92.45
3	87.67	86.82	87.34	86.06	93.45
4	86.45	87.42	93.45	85.66	84.18
5	87.34	77.53	91.57	87.01	93.45
6	89.79	80.27	91.68	87.57	93.45
7	88.74	86.45	80.27	81.21	91.57
8	86.85	89.24	86.45	91.53	91.68
9	87.89	89.87	87.34	92.48	93.22
Mean	87.61	85.14	87.2	87	91.78
SD	1.09	4.17	4.68	3.35	2.94
K10 protocol					
1	88.87	95.16	85.81	91.27	98.01
2	90.15	95.44	85.68	93.16	98.99
3	84.45	89.63	86.06	86.62	99.28
4	92.02	90.6	85.66	87.13	97.84
5	92.78	88.59	87.01	88.54	96.93
6	86.45	92.11	87.57	88.92	98.01
7	80.19	92.71	81.41	90.27	98.67
8	81.79	93.24	91.53	90.54	97.89
9	82.82	93.71	91.43	91.82	96.93
Mean	86.61	92.35	86.9	89.8	98.06
SD	4.58	2.36	3.11	2.17	0.81

$$RR = 2806 * \left(\frac{105080}{47 * 60750} \right) = 103.26$$

$$\mathrm{OR} = 2806 * \left(\frac{105033}{47 * 57944} \right) = 108.219$$

Here, we can observe

$$\mathrm{OR} \approx RR$$

i.e. the values obtained for OR and RR for malaria cases are approximately similar, showing that we have a low dissimilarity in malaria classifications between the actual number of cases and the predicted number of cases used to identify malaria-prone zones. This validates the hypothesis and demonstrates the superior performance of ISI-BPNN.

8.2. Validation on thoracic data

The Thoracic Surgery dataset is multivariate, and the attributes are an integer and a real number. The data are from primary lung cancer patients who underwent major lung resections. The dataset is related to patients who survived for one or more years after the operation, and life expectancy is used as the class in the dataset. Patients who survived for one or more years are classified as True (T) and patients who did not survive as False (N).

8.3. Validation on Parkinson's dataset

The Parkinson's dataset contains values of biomedical voice measurements of patients with

Table 5. Improvements (%) in ISI-BPNN

Model Protocol	IFN	GCNN	SVM	MLP
K2	5.6	9.7	7.7	4.7
K10	9.19	9.2	6.18	11.9
Mean	7.39	9.45	6.94	8.3
SD	2.54	0.35	1.075	5.09

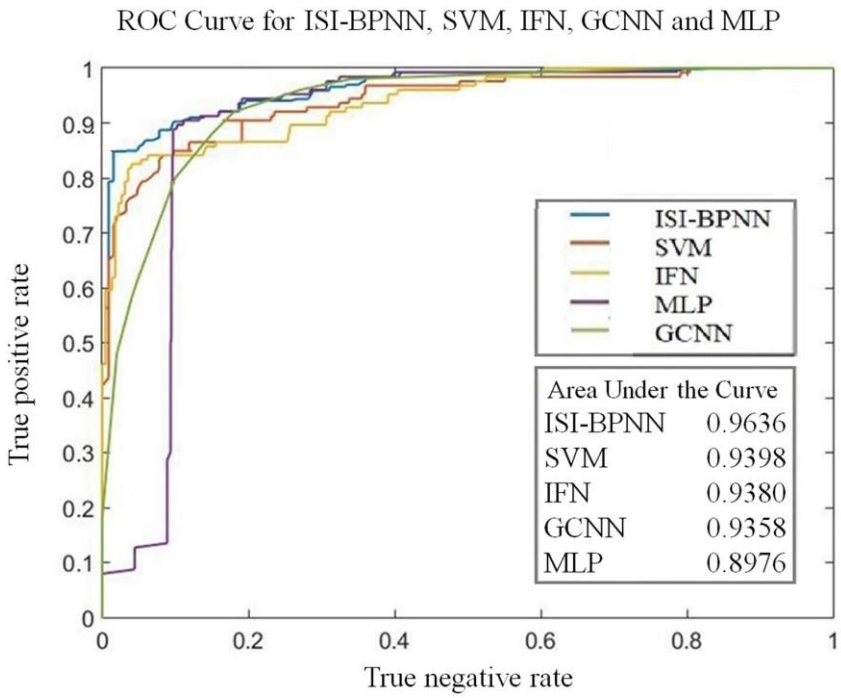

Figure 12. ROC curve and corresponding area under the curve

Parkinson's disease. There are 23 records of Parkinson's disease among the 31 records in the dataset. The dataset consists of 23 attributes and 197 instances, and is a multivariate dataset containing real attributes that are specifically used for classification problems. This was originally used in a feature selection method for voice disorders using recorded speech signals. The improvement shown by ISI-BPNN in comparison with conventional classifiers on the Thoracic Surgery and Parkinson's datasets for the K2 and K10 protocols is given in Table 9. The comparative analysis of validation datasets is shown in Figure 17.

Experiments were carried out to test the robustness and validate the proposed method using the Thoracic Surgery and Parkinson's datasets. The average accuracy for the Thoracic Surgery dataset for the K2 protocol was found to be **0.7588**, and for the K10 protocol, this was **0.8236**; the average accuracy for the Parkinson's dataset for the K2 protocol was found to be **0.8175,** and for the K10 protocol, this was **0.8818,** as represented below in Figure 18.

The improvements offered by ISI-BPNN over conventional classifiers on these two datasets were found to be **11.4%** for the Thoracic Surgery dataset and **6.05%** for the Parkinson's dataset. These values show that if the size of the training dataset is increased, the accuracy of the system is high compared with the smaller dataset provided

Table 6. Sample dataset

WN	T_{max} (°C)	T_{min} (°C)	Humidity (%)	Rainfall (mm)	# patients
1	30	17	55	3	52
2	30	17	56	4	62
3	31	17	55	14	45
4	32	18	62	12	45
5	33	19	60	5	32
6	34	20	58	31	48

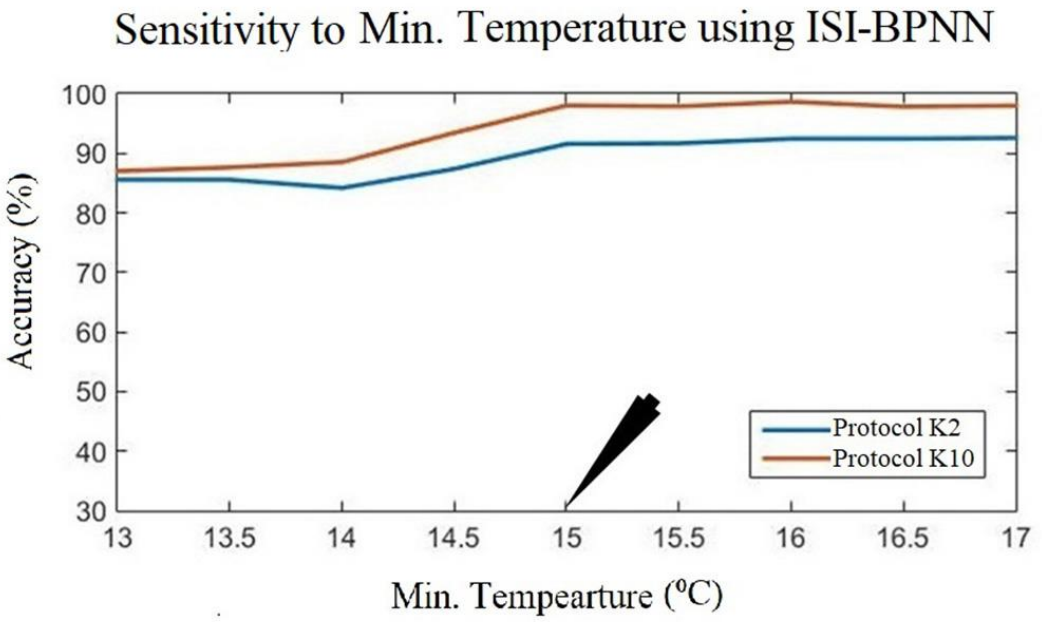

Figure 13. Sensitivities to minimum temperature

during execution. In the K2 protocol, half of the data are used for training and the other half for testing, giving lower accuracy for both datasets compared to the K10 protocol, where 90% of the data are used for training and 10% for testing. Thus, the proposed method is validated against two datasets.

We trained ISI-BPNN using the training data, and then used the testing data to generate predictions. This process was repeated with the MLP, GCNN, SVM, and IFN schemes. Table 9 shows the results using the proposed method and other existing methods such as MLP, IFN, SVM and GCNN using K10. We can easily see that ISI-BPNN outperforms the other models, giving accuracies of **89.93%**, **98.67%**, and **99.28%** for monthly and yearly data and historical data over three years.

To validate the proposed methodology, we performed these tests on two more datasets called Parkinson's and Thoraric Surgery, retrieved from the UCI Repository. The results are shown in Table 10. After every round, the dataset was shuffled and the protocol was applied. The results obtained from these validation experiments shows that the accuracy of ISI-BPNN increases as the size of the training dataset.

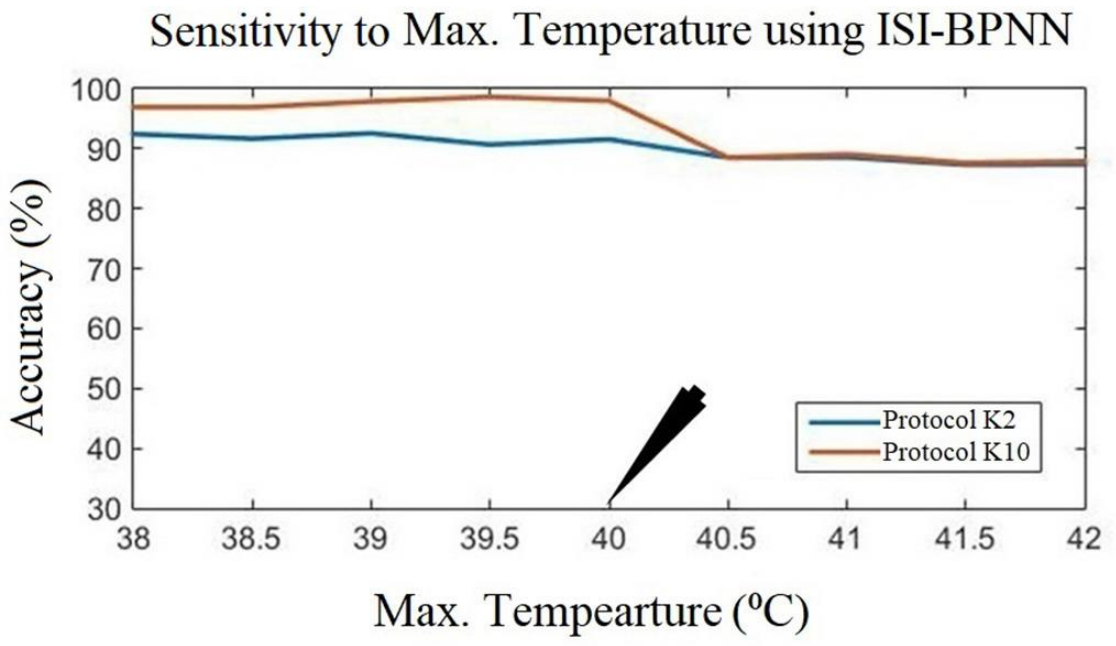

Figure 14. Sensitivities to maximum temperature

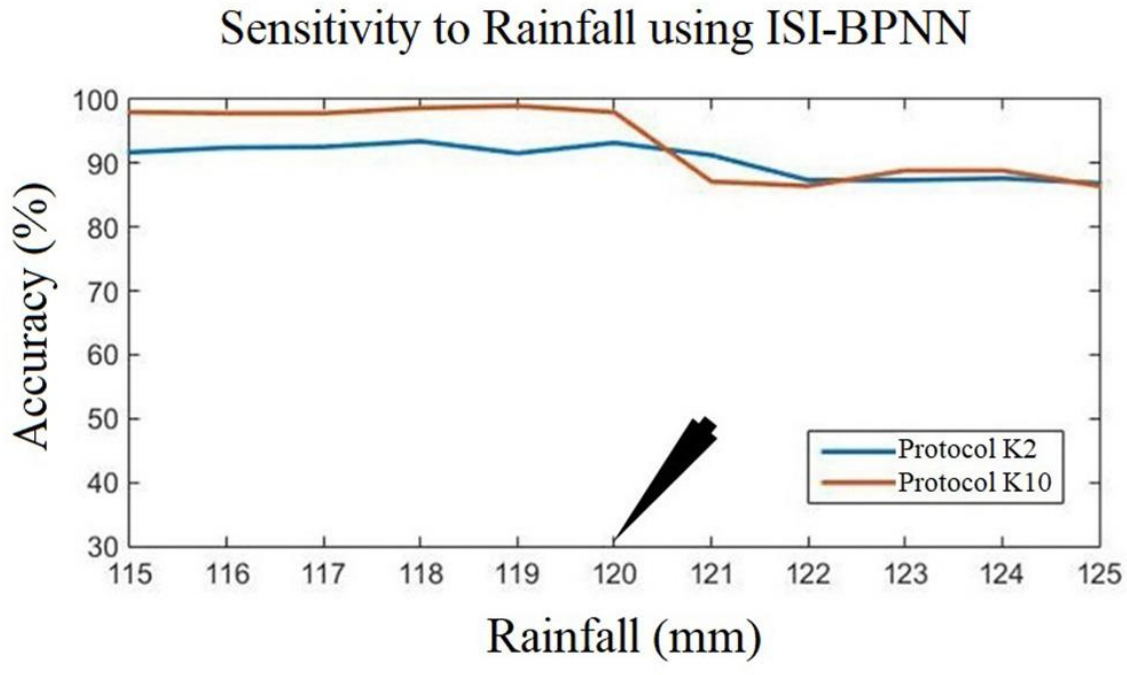

Figure 15. Sensitivities to rainfall

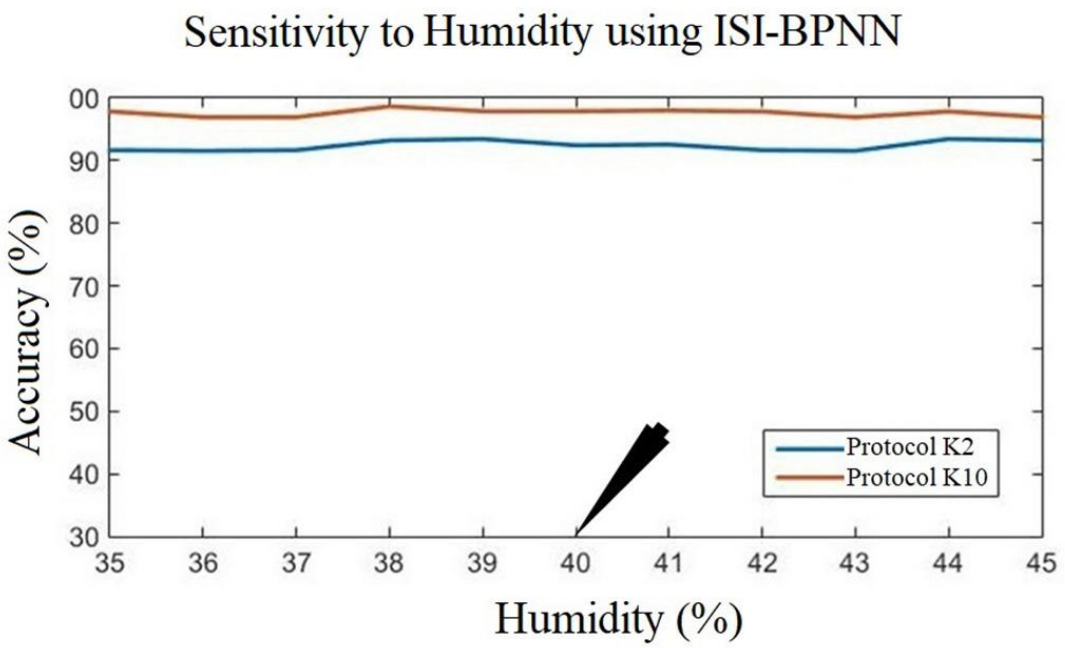

Figure 16. Sensitivities to humidity

Table 7. Standard deviation in classifiers for parameters.

CL Prm	MLP	SVM	IFN	GCNN	ISI-BPNN
T_{max}	2.92	2.36	2.17	3.35	2.13
T_{min}	3.56	4.17	3.11	2.17	3.52
Rainfall	2.44	2.89	2.85	2.19	2.61
Humidity	1.35	1.7	0.59	1.92	0.58

9. DISCUSSION

In this study, we proposed a new spiking function embedded in the BPNN framework called ISI-BPNN, which was applied to predict the occurrence of malaria disease in different geographical regions of Goa. The sensitivity of ISI-BPNN towards metrological factors was analyzed. The model was benchmarked against a set of four conventional classifiers: MLP, IFN, SVM, and GCNN. ISI-BPNN showed superior performance, yielding a cross-validation accuracy of **93.22%** using K2 (50% training) and **99.28%** using K10 (90% training). Our benchmarking results showed an improvement of **11.9%** against an MLP and **9.19%** against IFN models. ISI-BPNN was also tested for reliability and stability. The hypothesis for the model was validated using the two synthetic datasets called Thoracic Surgery and Parkinson's. The results showed very low deviation (<5%), thus demonstrating the robustness of the model. The study was carried out on a system with the following specifications: 8 GB RAM, Intel® Xeon® CPU E5-2620 v4@ 2.10 GHz, 64-bit operating system, x64-based processor, using the software application MATLAB R2015a.

We performed this study using data for the western coastal regions of India, where the population index is low compared with the northern regions and the local flora and other metrological indices are very different. These coastal areas are very suitable for the survival of malaria-carrying

Table 8. Odds Ratio table

Odds Ratio Index	Diseased	Healthy
Exposed	2806	57944
Non exposed	47	105033

Table 9. Classifier accuracies (%) in K2 and K10

Protocol	SVM	MLP	IFN	GCNN	ISI-BPNN
K2	85.14	86.61	86.91	83.14	91.78
K10	92.35	87.61	89.81	87	98.06
Average	88.75	87.11	88.36	85.07	94.92
SD	5.09824	0.707107	2.05061	2.729432	4.440631

parasites. Based on the relevant metrological and environmental factors, we prepared the model to predict the incidence of malaria. Malaria is a major problem in India and its neighboring countries, this study is an attempt to model an Indian region to propose a model which can identify malaria-free zones in India. A target of the WHO is to make India malaria-free by 2030, and support for this study was provided by the Indian Government, with the aim of researching public epidemics and healthcare and preventing the spread of this life-threatening diseases. In the future, this work will be extended and used to eliminate malaria to meet the goal of zero cases of this disease.

Validation protocols like segregation analysis were applied to the obtained results, and we can see that the proposed model outperforms existing methods. Better prediction results and higher accuracy are obtained as the data size is increased; if the training dataset is small, the accuracy is low and when we increase the size of the training dataset, the accuracy increases to a satisfactory level. The performance of the proposed method is also evaluated using malaria data. Monthly, half-yearly data, annual and five-year combined data are used for this performance evaluation. A workflow model is given in Figure 2, and this illustrates the process of this study. Firstly, the collected data were preprocessed and missing values cleaned. The dataset was divided into training and testing data according to the K-fold technique; here, 10-fold cross-validation (10 CV or K10) and 2-fold cross-validation (2 CV or K2) were carried out. We considered several estimation parameters such as the accuracy and stability over the datasets. The dataset was shuffled using the 10-CV method (which uses 90% data for training and 10% for testing) and the 2-CV method (50% data for training and 50% data for testing). The performance evaluation phase of the proposed system gives very interesting results, as shown above. A segregation analysis is also performed to test the similarity and dissimilarity index of the model. For each village in Ponda, the value of the dissimilarity (out of 100) is obtained as follows: 5.49 for Cundaim, 5.009 for Querim, 4.880 for Adcolna, 4.255 for Ponchawadi, 5.653 for Durbhat, 3.204 for Codar, 5.213 for Niranchal and 3.363 for Siroda. In these experiments, we used data from 2014 and 2015 for training and 2016 data for testing. From the above dissimilarity index analysis, we conclude that the villages of Siroda, Codar, Ponchawadi, Adcolna and Niranchal have an accuracy close to 97%, and thus are prone to malaria. If we consider Ponda as an overall location, we need to find the total population and the total number of cases in all the villages of Ponda; this gives the total population of Ponda as 165,830 including both urban and rural areas, and the number of malaria cases is found to be around 2,853 from entire dataset. Using these values in the evaluation, we obtained a dissimilarity index of 5.670 for the entire Ponda location, with a ground similarity of about 94.30. We can conclude that the Ponda area is not malaria-prone, because there was a decrease in the average number of malaria patients in 2016

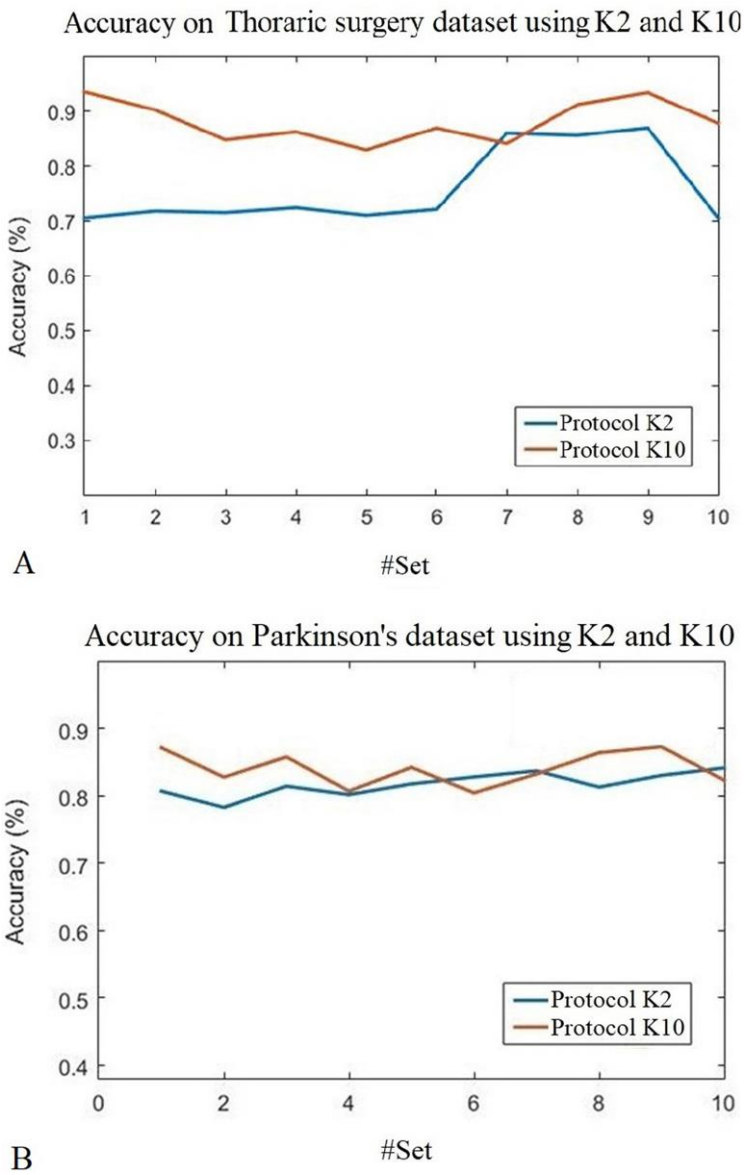

Figure 17. Validation accuracy for the dataset (a) Thoracic Surgery and (b) Parkinson's

compared to 2014 and 2015. In addition to the dissimilarity index, we also computed the isolation and exposure indices and showed that the ISI-BPNN exhibits very low dissimilarity to the number of actual and predicted malaria cases.

9.1. Benchmarking

The benchmarking study and comparative analysis is shown in chronological order, and the attributes are depicted in the columns of the Table 11. As can be observe, none of the previous studies applied the CV protocol (see column C6). Although many authors have worked on malaria disease, most have used laboratory data from blood samples, and have classified malaria-infected and healthy cells. These authors have also included malaria parasite and species data to identify the disease in their study. In some of these studies, metrological data were also used. In the present study, we focused on

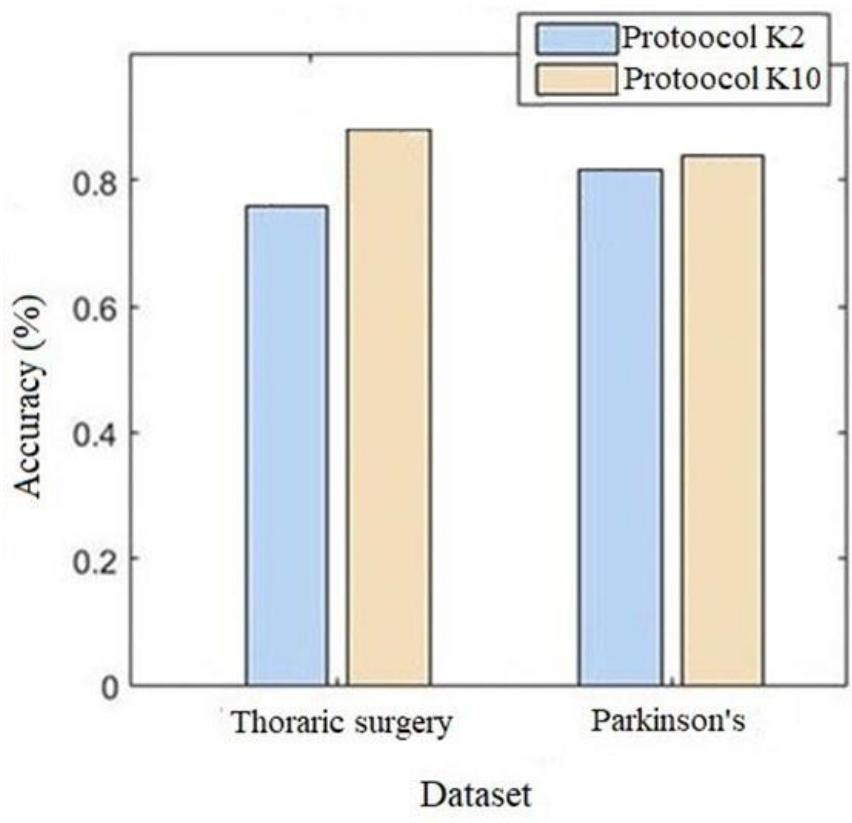

Figure 18. Bar representation of accuracies for two datasets (numbers on the bar are standard deviation)

metrological data and obtained malaria data from a regional government hospital. Scientific validation is given in column C7. The proposed method exhibits better accuracy than other methods (see column C9). As completely different approaches have been developed over the last ten years, many experiments have been carried out to achieve the present state of the art. However, despite the large variety of studies, current performance is not satisfactory for clinical use. Several prior articles simply discuss the sensitivity and specificity of classification, representing just one in operation purpose on a receiver in operation characteristic. Some publications aim to identify the progress and control status, which may add an additional complete analysis of any technique for various sensitivity necessities.

Austeclino *et al.* (33) used immunological and epidemiological data and the past infection history of the patient for malaria diagnosis. An ANN and a Bayesian network (BN) were used with a comparison of the classification (diagnosis) results using light microscopy and polymerase chain reaction (PCR) laboratory methods. The authors reported improvements in accuracy of 18.75% and 6.25% for the ANN and BN, respectively, compared with microscopic laboratory tests. Memeu *et al.* (36) developed a method of identification of parasite life stages using blood smear images. These authors used an ANN for the classification of infected erythrocytes in different stages of the parasite life cycle. The results showed an accuracy of identification of species of the plasmodium family of 96.3%. Chavan *et al.* (35) used image processing method for malaria screening involving an SVM-based classifier, and used a gray-level co-occurrence matrix to extract features from RBC colored images (later converted to grayscale) which were used as input to an SVM and an ANN. These authors

Table 10. Validation of ISI-BPNN in validation data

Protocol Shuffled set	Thoraric Surgery		Parkinsons	
	K2	K10	K2	K10
set1	0.7057	0.8019	0.8071	0.9357
set2	0.7181	0.8179	0.7829	0.9031
set3	0.7153	0.8282	0.8145	0.8484
set4	0.7243	0.8071	0.8019	0.8631
set5	0.7104	0.8126	0.8179	0.8301
set6	0.7213	0.8045	0.8282	0.8698
set7	0.8606	0.8027	0.8374	0.8418
set8	0.8566	0.8645	0.8131	0.9126
set9	0.8701	0.8734	0.8306	0.9345
set10	0.7059	0.8235	0.8418	0.8789
Average accuracy	0.7588	0.8236	0.8175	0.8818
Standard Deviation	0.0718	0.0255	0.0177	0.0379

obtained classification accuracies of 98.25% and 78.53% for SVM and ANN, respectively. Chiroma *et al.* (24) discussed the classification of malaria using thin and thick blood smears with a Jordan-Elman neural network (recurrent neural network). These authors achieved a classification accuracy of 96.4%. Vijeta *et al.* (34) performed prediction of malaria outbreaks using SVM and ANN as data mining classifiers, and obtained RMSE values of 0.12 and 0.47, respectively, i.e. with superior performance from the SVM. Purnima *et al.* (31) developed an ANN-based classifier for the binary classification of red blood cells (infected vs. normal) taken from holographic images. This system was trained on the quantitative features derived from the cellular images, and demonstrated an accuracy of 90%. Rahila *et al.* (30) used the patient's medical history (including shivering, vomiting, dry cough, back pain and headache) and symptoms as input to the MLP and performed malaria classification as positive or negative. Authors used backpropagation, backpropagation with momentum and a resilient propagation learning rule for MLP training, and obtained a classification accuracy of 85% in the backpropagation learning method. Santosh *et al*. (12) presented an ANN that used a sigmoid function as an activation function for a prediction model for the prevalence of malaria using big data processing; this was applied to the southern regions of India, and addressed the problem of scalability and time complexity for traditional machine learning algorithms. Belay (32) applied a support vector regression (SVR) and ANN in the classification of malaria data. The results showed values of root mean square error (RMSE) of 4.29 and 5.57, respectively, for the SVR and ANN. In the proposed method, we develop a new spiking function and obtain the ISI, which is aggregated and used as an input to the sigmoid function. The new sigmoid function is also used as an activation function in the backpropagation algorithm, and is called ISI-BPNN. Metrological factors are used as input data for the number of malaria cases within a particular geographical location. We also used K2 and K10 K-fold validation protocols, where we achieved accuracies of 88.09% and 98.67% for K2 and K10, respectively.

9.2. A Special note on the sigmoid function

The sigmoid function is an activation function used in a backpropagation algorithm. As the input to the conventional sigmoid function is replaced in the proposed model with an aggregated spiking function, the protocol is known as ISI-based backpropagation. The new sigmoid function plays a vital role in the system dynamics. Once all these analytical studies performed, we can see from many points that, the developed model is obtaining its goal. The hypothetical system used for the development of this model was

Table 11. Benchmarking against previous results in the literature

RN	C1	C2	C3	C4	C5	C6	C7	C8	C9
	Works	Data types	Classifier types	Feature types	# Features	K-fold CV*	Scientific validation	Data size	Accuracy (%)
R1	(33)	Laboratory data	Bayesian net	Environmental variables, clinical treatments	7	N+	Y#	580	80%
R2	(36)	Malaria species data	MLP	Color, morphological, texture	-	N+	N+	205	90.34%
R3	(35)	Laboratory data	SVM, MLP	Images	-	N+	N+	140	87.8%
R4	(24)	Blood smear	Jordan-Elman NN	-	6	N+	Y#	450	96.4%
R5	(34)	Metrological data	SVM, MLP	Environmental variables	6	N+	Y#	1680	89%
R6	(31)	Laboratory data	MLP	RBC samples, images	6	N+	N+	48	90%
R7	(30)	Laboratory data	MLP	Blood samples, symptoms	-	N+	Y#	376	85%
R8	(12)	Clinical and metrological data	MLP	Environmental variables, clinical treatments	5	N+	Y#	52	80%
R9	(32)	Laboratory data	MLP	-	5	N+	Y#	-	87%
R10	Proposed work	Metrological data	ISI-BPNN	Environmental variables	4	K2	Y#	4744	88.09%
R11	Proposed work	Metrological data	ISI-BPNN	Environmental variables	4	K10	Y#	4744	98.67%

*CV – Cross-validation, RN – Row number, #Authors used the method, +Authors did not used method

evaluated using several measures, and those measures were justified by tests and analysis. One of the major factors in the success of the developed model is a lower computational complexity due to the spiking sigmoid function. The developed model has a lower order of computational function, making it faster and less complex than legacy models. Another factor is the use of K-fold protocols for shuffling the data during computation, which makes the system more reliable in terms of the different sizes of data inputs. We observed that for a smaller training dataset, the prediction accuracy was poor, but when of the size of the test dataset was increased, the accuracy increased. For the larger training set, the accuracy was about 99.28%, as shown in the benchmarking study. The learning behavior of the system is similar to the natural neurons in the human brain; as more knowledge is obtained, performance increases. In the same way, the accuracy of the proposed method is higher for larger training samples. From this point of view, we have achieved our goal of learning and developing a biological neuron model.

9.3. A Note on spiking neuron models

Neural networks are often used for classification and regression tasks. Feng *et al.* (25,26) discussed IFN models with current inputs as part of a development series of third-generation neural networks. A neuron model was trained and applied to a binary classification (zero or one) equivalent to XOR gates. A spike was generated if the voltage was greater than a threshold when the current was applied to an R-C circuit. Mishra *et al.* (22) applied single and quadratic IFN models to the binary classification of an XOR problem (similar to Feng *et al.* (25)) and to a linear regression-based classification. Wulfram *et al.* (27) showed mathematically that a single neuron can be used for classification, and referred to this as the plasticity phenomenon. Chandra *et al.* (28) presented a new neuron model similar to quadratic IFN for classification, using a lower-order activation function, and demonstrated a reduction in computational complexity. Schollas *et al.* (29) presented the modeling of bio-inspired neural network and applied to time domain beamforming, model was used for

sonar ranging, focusing and steering. This work was influenced by two contributions from Yadav *et al.* (13) and Chandra *et al.* (28), in which a new spiking model was presented by the authors.

9.4. Strengths, weaknesses and extensions

It can be observed that ISI-BPNN performs better in terms of prediction. Due to the use of a lower-order function, the model has a lower computational complexity than traditional models; as the size of the dataset and the number of iterations are increased, the proposed model performs faster, and the time complexity is lower. The scope of this experiment is limited to numerical types of data, and a limited amount of collected data is used. We can use this system for a broad range of datasets, and can extend the model to add more features such as the ratio of vegetation, water index, geographical area and population index to achieve better results. This model can also be applied to different datasets for the early prediction of disease. Based on our results, it is evident that our model can be used as an early predictor for malaria for epidemic-prone regions. We could also adapt fuzzy rule sets to give more robustness to the system. Through this study, we can serve public epidemic healthcare and prevent the spread of life-threatening diseases by the early prediction of disease. In future, this work will be extended to help ensure the goal of zero cases of malaria.

10. CONCLUSIONS

This study has presented an ISI-based BPNN (ISI-BPNN) architecture that uses a single-pass spiking learning strategy with a parallel structure that is useful for nonlinear regression tasks. We demonstrated that ISI-BPNN was more efficient than the MLP, IFN, SVM, and GCNN models. A malaria dataset was collected through the National Institute of Technology, Goa. The results demonstrated that ISI-BPNN shows superior performance, yielding a cross-validation accuracy of **93.22%** for K2 (50% training data) and **99.28%** for K10 (90% training data). Our benchmarking results showed an improvement of **11.9%** against the multilayer perceptron and **9.19%** against IFN models. ISI-BPNN was also tested for its reliability and stability. Our proposed ISI-BPNN model effectively predicted the class of malaria-prone regions as high or low risk for consecutive years. In future, ISI-BPNN could be extended to the prediction of malaria-prone areas in other Indian states and worldwide. This model could also be extended to the prediction of diseases in different geographical locations. We conclude that spiking model found to be efficient than classical neuron models for classification.

11. ACKNOWLEDGMENT

We are thankful to the Department of Science and Technology, Science and Engineering Research Board, New Delhi, India vide, Project No. ECR/2017/001074, for financial support. We also thank Dr. Pradip Shinkre, Medical Superintendent, SDH, Ponda for providing data used in this study and Dr. Ashwani Kumar, Scientist-F & Officer-In-Charge, National Malaria Research Institute, Goa for his key suggestions to carry out the research. Special thanks to Global Biomedical Technologies, Inc., Roseville, CA, USA in support throughout the project, especially in experimental design, performance evaluation and stability analysis.

12. REFERENCES

1. World Health Organization: Global technical strategy for malaria 2016-2030. World Health Organization, (2015)

2. World Health Organization: World malaria report. World Health Organization, (2018)

3. Ashwani Kumar, Neena Valecha, Tanu Jain, Aditya P. Dash: Burden of malaria in India: retrospective and prospective view. The American journal of tropical medicine and hygiene 77, No. 6_Suppl, 69-78 (2007)
DOI: 10.4269/ajtmh.2007.77.69

4. Wernsdorfer Walther: Global challenges of changing epidemiological patterns of malaria. Acta tropica 121, No. 3, 158-165 (2012)

DOI:
10.1016/j.actatropica.2011.06.014

5. Esther Love Darkoh, John Aseidu Larbi, Eric Adjei Lawer: A weather-based prediction model of malaria prevalence in ameni west district, Ghana. Malaria research and treatment (2017)
DOI: 10.1155/2017/7820454

6. Aparup Das, Anupkumar R. Anvikar, Lauren J. Cator, Ramesh C. Dhiman, Alex Eapen, Neelima Mishra, Bhupinder N. Nagpal, Nutan Nanda, Kamaraju Raghavendra, Andrew F. Read, Surya K. Sharma, Om P. Singh, Vineeta Singh, Photini Sinnis, Harish C. Srivastava, Steven A. Sullivan, Patrick L. Sutton, Matthew B. Thomas, Jane M. Carlton, Neena Valecha: Malaria in India: the center for the study of complex malaria in India. Acta tropica 121, No. 3, 267-273 (2012)
DOI:
10.1016/j.actatropica.2011.11.008

7. Joan H Bryan, Desmond H Foley, Robert W Sutherst: Malaria transmission and climate change in Australia. The Medical Journal of Australia 164, No. 6, 345(1996)

8. K Negash, A Kebede, A Medhin, D Argaw, O Babaniyi, J O Guintran, C Delacollette: Malaria epidemics in the highlands of Ethiopia. East African medical journal 82, No. 4 (2005)
DOI: 10.4314/eamj.v82i4.9279

9. Linhua Tang: Progress in malaria control in China. Chinese medical journal 113, No. 1, 89-92 (2000)

10. L. J. Bruce-Chwatt, B. A. Southgate, C. C. Draper: Malaria in the United Kingdom. British Medical Journal 2, No. 5921, 707 (1974)
DOI: 10.1136/bmj.2.5921.707

11. Narla Mohandas, An Xiuli: "Malaria and human red blood cells." Medical microbiology and immunology 201, no. 4, 593-598 (2012)
DOI: 10.1007/s00430-012-0272-z

12. Santosh Thakur, Ramesh Dharavath: Artificial neural network based prediction of malaria abundances using big data: A knowledge capturing approach. Clinical Epidemiology and Global Health (2018)
DOI: 10.1016/j.cegh.2018.03.001

13. Abhishek Yadav, Mishra Deepak, R. N. Yadav, Sudipta Ray, Prem K. Kalra: Learning with single integrate-and-fire neuron. In Neural Networks, 2005. IJCNN'05. Proceedings. 2005 IEEE International Joint Conference on, vol. 4, 20052156-2161 (2005)

14. Warren S. McCulloch, Walter Pitts: A logical calculus of the ideas immanent in nervous activity. The bulletin of mathematical biophysics 5, No. 4, 115-133 (1943)
DOI: 10.1007/BF02478259

15. Andrew A. Sharp, L. F. Abbott, Eve Marder: Artificial electrical synapses in oscillatory networks. Journal of neurophysiology 67, no. 6, 1691-1694 (1992)
DOI: 10.1152/jn.1992.67.6.1691

16. Eugene M Izhikevich: Resonate-and-fire neurons. Neural networks 14, no. 6-7, 883-894 (2001)
DOI: 10.1016/S0893-6080(01)00078-8

17. Abbott Larry: Lapicque's introduction of the integrate-and-fire model neuron

(1907). Brain research bulletin 50, No. 5-6, 303-304 (1999)
DOI: 10.1016/S0361-9230(99)00161-6

18. Abbott Larry, Carl van Vreeswijk: Asynchronous states in networks of pulse-coupled oscillators. Physical Review E 48, No. 2, 1483 (1993)
DOI: 10.1103/PhysRevE.48.1483

19. Richard B. Stein: A theoretical analysis of neuronal variability. Biophysical Journal 5, No. 2, 173-194 (1965)
DOI: 10.1016/S0006-3495(65)86709-1

20. Nicolas Brunel, Peter E. Latham: Firing rate of the noisy quadratic integrate-and-fire neuron. Neural Computation 15, No. 10, 2281-2306 (2003)
DOI: 10.1162/089976603322362365

21. Nicolas Fourcaud-Trocmé, Hansel David, Van Vreeswijk Carl, Brunel Nicolas: How spike generation mechanisms determine the neuronal response to fluctuating inputs. Journal of Neuroscience 23, No. 37, 11628-11640 (2003)
DOI: 10.1523/JNEUROSCI.23-37-11628.2003

22. Deepak Mishra, Abhishek Yadav, Prem K. Kalra: Learning with single quadratic integrate-and-fire neuron. In International Symposium on Neural Networks, Springer, Berlin, Heidelberg, 424-429 (2006)
DOI: 10.1007/11759966_63

23. Eugene M Izhikevich: Simple model of spiking neurons. IEEE Transactions on neural networks 14, No. 6, 1569-1572 (2003)
DOI: 10.1109/TNN.2003.820440

24. Haruna Chiroma, Sameem Abdul-kareem, Umar Ibrahim, I. Gadam Ahmad, Abdulmumini Garba, Adamu Abubakar, M. Fatihu Hamza, and T. Herawan: Malaria severity classification through Jordan-Elman neural network based on features extracted from thick blood smear. Neural Network World 25, No. 5, 565 (2015)
DOI: 10.14311/NNW.2015.25.028

25. Jianfeng Feng, Guibin Li: Integrate-and-fire and Hodgkin-Huxley models with current inputs. Journal of Physics A: Mathematical and General 34, No. 8 1649 (2001)
DOI: 10.1088/0305-4470/34/8/311

26. Jianfeng Feng , Yunlian Sun , Hilary Buxton , Gang Wei: Training integrate-and-fire neurons with the Informax principle II. IEEE Transactions on Neural Networks 14, No. 2, 326-336 (2003)
DOI: 10.1109/TNN.2003.809419

27. Wulfram Gerstner, Werner M. Kistler: Spiking neuron models: Single neurons, populations, plasticity. Cambridge university press, (2002)
DOI: 10.1017/CBO9780511815706

28. Bala Chandra, KV Naresh Babu: A new spiking neuron model. In Neural Networks (IJCNN), The 2013 International Joint Conference on, 1-5 (2013)
DOI: 10.1109/IJCNN.2013.6706930

29. Michae Scholles, B. J. Hosticka, M. Kesper, P. Richert, M. Schwarz: Biologically-inspired artificial neurons: modeling and applications. In Neural Networks, 1993. IJCNN'93-Nagoya. Proceedings of 1993 International Joint Conference on, vol. 3, 2300-2303 (1993)

30. Rahila Parveen, Akhtar Hussain Jalbani, Mohsin Shaikh, Kashif Hussain Memon, Saima Siraj, Mairaj Nabi, Shamshad Lakho: Prediction of Malaria using Artificial Neural Network. International Journal of Computer Science and Network Security 17, No. 12, 79-86 (2017)

31. Purnima Pandit, A. Anand: Artificial Neural Networks for Detection of Malaria in RBCs. arXiv preprint arXiv, 1608.06627 (2016)

32. Enyew Belay: Exploration of artificial neural network and support vector regression for malaria incidence prediction in amhara region, Ethiopia. International Journal of Current Advanced Research, Volume 7; Issue 5(J), 12875-12879 (2018)

33. Austeclino Magalhães Barros Júnior , Angelo Amâncio Duarte, Manoel Barral Netto, Bruno Bezerril Andrade: Artificial Neural Networks and Bayesian Networks as supporting tools for diagnosis of asymptomatic malaria. In e-Health Networking Applications and Services (Healthcom), 12th IEEE International Conference on, 106-111 (2010)

34. Vijeta Sharma, Ajai Kumar, L. Panat, Ganesh Karajkhede, and A. Lele: "Malaria outbreak prediction model using machine learning." Int. J. Adv. Res. Comput. Eng. Technol 4, 4415-4419 (2015)

35. Sneha Narayan Chavan, Ashok Manikchand Sutkar: Malaria disease identification and analysis using image processing. Int. J. Latest Trends Eng. Technol 3, 218-223 (2014)

36. Daniel Maitethia Memeu, Kenneth Amiga Kaduki, A. C. K. Mjomba, Njogu Samson Muriuki, Lucy Gitonga: Determination of Plasmodium Parasite Life Stages and Species in Images of Thin Blood Smears Using Artificial Neural Network. Open Journal of Clinical Diagnostics 3, No. 04, 183 (2013)
DOI: 10.4236/ojcd.2014.42014

37. Frank Rosenblatt: Principles of neurodynamics, perceptrons and the theory of brain mechanisms. Cornell Aeronautical Lab Inc Buffalo NY, No. VG-1196-G-8 (1961)
DOI: 10.21236/AD0256582

38. Corinna Cortes, Vladimir Vapnik: Support-vector networks. Machine learning 20, no. 3, 273-297 (1995)
DOI: 10.1007/BF00994018

39. Bao-Gang Hu, Han-Bing Qu, Yong Wang, Shuang-Hong Yang: A generalized-constraint neural network model: Associating partially known relationships for nonlinear regressions. Information Sciences 179, No. 12, 1929-1943 (2009)
DOI: 10.1016/j.ins.2009.02.006

Abbreviations: IFN: Integrate and Fire Neuron, BP: Backpropagation, SNN: Spiking Neural Network, ISI: Interspike Interval, CV: Cross Validation, DC: Dataset Combination, CN: Combination Number, WN: Week Number, GCNN: Generalized Constraint Neural Network, MLP: Multilayer Perceptron, SVM: Support Vector Machine, BPNN: Backpropagation Neural Network.

Key Words: Malaria, Integrate-And-Fire Neuron, Backpropagation, Spiking Neural Network, Interspike Interval, Machine Learning Algorithm, Performance

Send correspondence to: Jasjit S. Suri,

Advanced Knowledge Engineering Centre, Global Biomedical Technologies, Inc. Roseville, CA, USA, Tel: 916-749-5628, Fax: 916-749-4942, E-mail: jsuri@comcast.net